EFI 78-29

FERMILAB-PUB-78-113-E

Production of hadrons at large transverse momentum in 200, 300 and 400 GeV p-p and p-N collisions.*

D. Antreasyan,† J.W. Cronin, H.J. Frisch, and M.J. Shochet

The Enrico Fermi Institute, and Department of Physics,

University of Chicago, Chicago, Illinois 60637

and

L. Kluberg,†† P.A. Piroué, and R.L. Sumner

Department of Physics, Joseph Henry Laboratories,

Princeton University, Princeton, New Jersey 08540

ABSTRACT

Measurements of the invariant cross section $Ed^3\sigma/d^3p$ are presented for the production of hadrons (π, K, p and $\bar{p}$) at large transverse momentum ($p_\perp$) by 200, 300, and 400 GeV protons incident on H_2, D_2, Be, Ti and W targets. The measurements were made at a laboratory angle of 77 mrad, which corresponds to angles near 90° in the c.m. system of the incident proton and a single nucleon at rest. The range in $p_\perp$ for the data is $0.77 \leq p_\perp \leq 6.91$ GeV/c, corresponding to values of the scaling variable $x_\perp = 2\, p_\perp/\sqrt{s}$ from 0.06 to .64. For p-p collisions, the pion cross sections can be represented in the region $x_\perp > .35$ by the form $\frac{1}{p_\perp^{\,n}}(1-x_\perp)^b$, with $n \simeq 8$ and $b \simeq 9$. The ratio of π^+ to π^- production grows as a function of $x_\perp$ to a value larger than 2 at $x_\perp \gtrsim .5$. The ratios of the production of K^+ and protons to π^+ and of K^- and anti-protons to π^- also scale with $x_\perp$ for p-p collisions. The $K^\pm$, p and $\bar{p}$ fitted values for n and b are given. Particle ratios are also presented for D_2, Be, Ti, and W targets and the dependences on atomic weight (A) are discussed.

I. INTRODUCTION

It is only very recently, with the advent of quantum chromodynamics (QCD), that models of large transverse momentum ($p_\perp$) behavior have had a fairly firm theoretical foundation.[1] Previously, several hard scattering models have each had striking partial successes, such as the predictions for the $x_\perp \equiv 2\ p_\perp/\sqrt{s}$ and $p_\perp$ dependences of the $\pi^\pm$, $K^\pm$, and p and $\bar{p}$ cross sections in the constitutent interchange model (CIM),[2] or the π^+/π^- ratio versus $x_\perp$ predicted by the Field-Feynman "black box" model.[3] However, in these older models there is a large ad hoc component.

The early single particle inclusive measurements made at the ISR[4] and Fermilab[5,6] have been important in this evolution. The difficulty of the multiparticle "jet" experiments on the one hand, and the strong theoretical motivation from the results of e^+e^- annihilation and from deep-inelastic lepton scattering on the other, have resulted in a great deal of theoretical analysis of the single particle measurements. It now appears that with a theory which actually predicts the single particle spectra to be rather complicated functions of $x_\perp$ and $p_\perp$, precise measurements over a wide range in these variables will again be important.

In this paper we summarize the results from a study at Fermilab of the production of hadrons at large transverse momentum. Some of these data have already been published, in particular the cross sections[7] and particle ratios[8] measured with H_2 and D_2 targets, and a brief summary of the atomic weight (A) dependence of the cross sections on D_2, Be, Ti and W targets.[9]

We have remeasured many of the nuclear cross sections published in an earlier Physical Review paper. The nuclear cross sections presented here have been measured with thinner targets of larger cross sectional area, and we feel they are systematically better measurements than the older ones. In particular, a problem, never understood in the older data, with the normalization between energies now seems to have been corrected.[7]

The experimental technique is simple and is thoroughly described in Ref. 5. In Section II, we briefly describe the spectrometer emphasizing the changes from that description. In Section III, we present and discuss the results for pion production in p-p and p-d collisions. Cross sections for p-"n" collisions derived from a subtraction of the p-p cross sections from the p-d cross sections are also given. The p-p cross sections are compared to those of the ISR. Data on the production of K^+, K^-, protons and anti-protons in p-p, p-d and p-"n" collisions are presented in Section IV. Section V contains cross section data for Be, Ti and W targets, and a discussion of their dependence on atomic weight (A). Section VI is a summary of our conclusions.

II. THE APPARATUS.

The apparatus used to make these measurements was located in the Proton East area of Fermilab. It consisted of a single-arm spectrometer located at an angle of 77 mrad with respect to the incident proton beam (see Fig. 1). For the production of relativistic ($\beta \simeq 1$) particles, this laboratory angle corresponds to 77°, 88° and 96° in the c.m. of a target nucleon at rest and a proton of incident energy 200, 300, or 400 GeV, respectively. Scintillation counter hodoscopes defined the particles' trajectories and measured the momenta to ±1%. Two 86-foot-long Cherenkov counters provided the particle identification.

The acceptance of the spectrometer, $d\Omega dp/p$, was 1.7×10^{-4} steradian-%. The spectrometer and the beam are described in detail in our earlier Physical Review paper,[5] and consequently only those details which are different will be discussed here.

A. The Hydrogen Target.

The hydrogen target consisted of an 8"-long, 1"-diameter Cu flask, with side walls 1/16" thick, and with .001"-thick hemispherical stainless steel end windows. The flask was cooled by a single loop of a liquid-He line which was soldered to the exterior of the flask. A 30"-long cryostat with .005"-thick Al end windows surrounded the flask. The assembly was at the end of a long transfer line so that the target could fit 15 feet inside the massive shielding of the Proton East target box.

Liquid hydrogen (or deuterium) was formed inside the flask by condensation when the flask was cooled by a 50-watt refrigerator located approximately 25' upstream of the target box. Carbon resistors indicated when the target was full. An external heat source was used to empty the target.

The target endured rates of up to 10^{13} protons/pulse, although data were not taken at rates above 5×10^{12} protons/pulse. Signs of boiling in the target were searched for by studying the counting rate versus beam intensity: no rate dependent effects were found at rates of up to 5×10^{12} protons/pulse, although the target could be inadvertently emptied (and was twice destroyed) by hitting the edge of the flask with a single pulse of the beam.

B. Target Empty Subtraction.

A target empty run was taken with every H_2 or D_2 run. The typical subtraction was about 10% for the p-p data and 5% for the p-d data. This is larger than one might expect from the small amount of material in the beam because the rates at large $p_\perp$ from the metal windows are enhanced by the anomalous A dependence of the cross sections.[5,9] Subtractions were done separately for each particle type π, K, or $p(\bar{p})$ at each value of $p_\perp$.

C. The Nuclear Targets.

In order to minimize possible thick target effects, the measurements presented in Ref. 5, obtained with targets of 0.2 interaction lengths, were repeated with thin targets of approximately 0.03 interaction lengths. The Be, Ti and W targets were each 1/4" square in cross section, and were 0.480 in., 0.341 in., and 0.131 in. long, respectively. The four nuclear targets were mounted on top of the LH_2 cryostat, and each target could be moved into the beam remotely. Data were taken with each target in turn to reduce systematic errors due to structure in the beam spill, targetting efficiencies, etc.

D. Low Transverse Momentum Runs.

In this experiment cross sections which span ten orders of magnitude have been measured. For low values of $p_\perp$, where the cross sections are large, there is a problem in that the counting rates become high. In the data taking and analysis described in Ref. 5, small scintillation counters were remotely moved into the spectrometer to decrease the solid angle subtended and thus the counting rate. Since then, changes made in the beam transport to the Proton Area at Fermilab allowed the beam intensity to be adjusted easily. Data were thus taken at all transverse momenta with the same trigger counters and hodoscopes.

III. RESULTS ON THE PRODUCTION OF π^+ AND π^- IN p-p, p-d, AND p-"n" COLLISIONS.

The results presented in this section have been summarized in a Physical Review Letter:[7] they are presented again for completeness. The invariant cross section $Ed^3\sigma/d^3p$ for pion production in p-p and p-d collisions at 200, 300, and 400 GeV are listed as a function of $p_\perp$ in Table I. The cross sections for π^- production are plotted versus $p_\perp$ in Fig. 2 for these three beam energies. The data have been corrected for decay-in-flight, nuclear absorption, and multiple scattering as described in detail in Ref. 5.

One additional correction that was not applied in Ref. 5 was made to the data presented here. The average transverse momentum accepted by the spectrometer depends on the slope of the production spectrum in the region of the spectrometer setting. Because of the energy dependence of the cross sections at large values of $p_\perp$, the slope, and hence the average value of $p_\perp$ accepted, is different at 200, 300, and 400 GeV. In the previous analysis the average accepted $p_\perp$ was calculated at 300 GeV and then was used also for the 200 and 400 GeV data. In this analysis the 200 and 400 GeV data have been corrected for this effect - the correction is negligible below $p_\perp \simeq 3$ GeV, and reaches a maximum of 8% at the largest measured values of $p_\perp$.

In addition to the statistical uncertainties in the cross sections we have assigned systematic errors of 5% everywhere except at the two lowest $p_\perp$ values where a 10% error has been included. We estimate the overall normalization is uncertain to 20% and the transverse momentum scale is uncertain to 1%. We estimate that the ratios of π^+ to π^- cross sections are uncertain to 10% due to possible systematic effects at all values of $p_\perp$.

It has long been the expectation that the inclusive production of high $p_\perp$ hadrons should scale as $Ed^3\sigma/d^3p = \frac{1}{p_\perp^4} f(x_\perp = 2p_\perp/\sqrt{s})$ at sufficiently high energies and $p_\perp$.[10] There are now explicit predictions[11] that the cross sections should behave as sums of terms each of the form $\frac{1}{p_\perp^n}(1-x_\perp)^b$. In the kinematic region we explore one term is expected to dominate. We have thus fitted the cross sections to a single such term.

We have calculated a least squares fit in the region $x_\perp \geq .35$. For the production of π^+, we find $n = 8.2 \pm .5$ and $b = 9.0 \pm .5$, with a χ^2 of 14.7 for 6 degrees of freedom (DOF). For π^-, we find $n = 8.5 \pm .5$ and $b = 9.9 \pm .5$, with a χ^2 of 2.1 for 6 DOF. Fits were also calculated for the regions $x_\perp \geq .30$ and $x_\perp \geq .40$, and the errors quoted above on b and n have been increased to include the results found with different fitting regions. The results for n and b are in good agreement with the predictions of the CIM model[2] of $n = 8$ and $b \simeq 9$. Fig. 3 shows the scaling properties of the π^+ and π^- cross sections versus $x_\perp$.

These values of n are also in good agreement with the original value of $n = 8.24 \pm 0.7$ obtained for π° production by the CCR collaboration[4] in p-p collisions at the ISR. Subsequent measurements of n by groups both at the ISR and Fermilab are listed in Table II.

A selection of single particle cross sections interpolated from ISR and Fermilab data for $p_\perp > 1.5$ GeV/c is shown on a global plot in Fig. 4. The data are for π° or the average of π^+ and π^- production near 90° in p-p collisions. Lines of constant cross section have been plotted on a two-dimensional plot of $p_\perp$ versus $(1-x_\perp)$. If a single term of the form $p_\perp^{-n}(1-x_\perp)^b$ dominates the form of the cross section, the data should lie on straight lines of slope n/b. The spacing between these lines in the ordinate is then $\frac{\log 10}{n}$, and in the abscissa is $\frac{\log 10}{b}$.

The solid lines drawn on the plot are an approximation to our data, and have n = 8.4 and b = 9.45. The dashed lines are the fit to the recent ISR data of Clark et al.[12] with n = 6.6 and b = 9.6.

The ratios of π^+ to π^- versus $p_\perp$ are presented in Table III. These ratios are plotted versus $x_\perp$ in Fig. 5; the dotted line is the QCD prediction of Feynman, Field and Fox.[13] The indication of a break in the theoretical curve at $x_\perp \simeq .3$ is predicted to be due to the crossover of gluon and valence quark fragmentation. The 200, 300, and 400 GeV data lie within statistics along a single curve versus $x_\perp$ as scaling predicts.

A naive procedure was employed to extract p-n invariant cross sections: the p-p cross sections were subtracted from the p-d cross sections presented in Table I. The π^+/π^- ratios for p-"n" as well as for p-p and p-d collisions are given in Table III and are shown in Fig. 5. The result is quite different from the p-p case: the possible droop at large $x_\perp$ may be due to the fact that at 400 GeV the spectrometer is not at 90° in the p-n c.m., and is in fact in the neutron (backward) hemisphere. Because the neutron has two d quarks and only one u quark, one might expect somewhat more π^- at large $x_\perp$.

IV. THE PRODUCTION OF K^+, K^-, p AND $\bar{p}$ IN p-p AND p-d COLLISIONS.

With the two 86-foot-long gas Cherenkov counters (see Ref. 5 for a detailed description), pion, kaon and proton cross sections were measured simultaneously. The data were reduced as ratios of kaons and protons to pions as this involved only the information from the Cherenkov counters, and are presented free from the normalization errors we have added to the cross sections.

Target empty subtractions were made separately for each particle type. The particle ratios were then corrected for decay-in-flight for the kaons and pions, and for the differences in nuclear absorption[14] for the different particle types as a function of momentum. The decay-in-flight correction, which for kaons ranged from a factor of 3.88 at $p_\perp$ = 0.77 to a factor of 1.15 at a $p_\perp$ of 6.91 GeV/c,was assigned a 10% error, which was combined in quadrature with the other errors. The correction for differential nuclear absorption, most significant for the $\bar{p}/\pi^-$ ratio at low momentum, amounted to less than 10%. Finally an overall 2% systematic uncertainty was included in the final error.

A word of caution with respect to the ratios and cross sections at lower values of $p_\perp$ is in order. Because the transformation from a fixed laboratory angle (in this case 77 mrad) to the c.m. frame depends on the velocity of the particle, the production angle at low values of $p_\perp$ for protons and anti-protons is different from that of pions measured at the same spectrometer setting. The production angles for protons and anti-protons for $p_\perp$ = 0.77, 1.16, 2.31, and 3.08 GeV are 125°, 106°, 99°, and 93°, respectively, at 300 GeV, while the respective pion angles are all 89°. Not knowing how to correct for this, we only warn the reader.

In Table IV we present the ratio of cross sections for $p/\pi^+(\bar{p}/\pi^-)$ for 200, 300, and 400 GeV protons incident on hydrogen and 400 GeV protons incident on deuterium. The corresponding data for the ratio K^+/π^+ (K^-/π^-) are listed in Table V. Figure 6 shows the ratios p/π and K/π versus $p_\perp$ for p-p collisions at the three incident proton energies.

Figures 7, 8, 9 and 10 compare our 300 GeV data with those of the British-Scandinavian Collaboration[15] obtained at the same energy ($\sqrt{s}$ = 23.4 GeV) and at 90° in the c.m. There is good agreement for the K/π ratios. However, our p/π^+

data are ~20% below theirs and the $\bar{p}/\pi^-$ ratios are lower by a factor of ~2 (see Figs. 9 and 10 for a comparison). We note that in our data the largest correction to the $\bar{p}/\pi^-$ ratio, the differential nuclear absorption correction, is less than 10%; however, the production angle is backward in the c.m. at low $p_\perp$.

If at high transverse momentum the invariant cross sections for all types of hadrons factor into a power of $p_\perp$ and a function of the scaling variable $x_\perp = 2p_\perp/\sqrt{s}$ (i.e., $Ed^3\sigma/d^3p = f(x_\perp)/p_\perp^n$), so should the ratios p/π^+, $\bar{p}/\pi^-$, and $K^\pm/\pi^\pm$. Using $f(x_\perp) = (1-x_\perp)^b$, a least squares fit in the region $x_\perp > 0.35$ gives the values for n and b presented in Table VI. The errors again have been increased as described in Section III.

These values for n and b correspond to the differences between the proton (or kaon) powers and those of the pion of the same charge. They are in good agreement with the predictions of the CIM[2] and of dimensional counting.[16] Figure 11 illustrates the scaling properties of these ratios.

Tables VII and VIII present the cross sections for K, p and $\bar{p}$ production in p-p and p-d collisions derived from the particle ratios and the pion cross sections of Table I. A naive estimate of the p-"n" cross sections and particle ratios can be made from these data.

V. HADRON PRODUCTION IN COLLISIONS OF 200, 300 and 400 GeV PROTONS WITH Be, Ti, and W TARGETS.

The original intention in our earlier work in having three nuclear targets with a wide range of atomic weight (A) was to be able to extrapolate to A=1. We felt, naively, that for the "hard" collisions only a single nucleon in the nucleus would be involved. It was therefore a surprise when we found that

although the cross sections did extrapolate as A^{α}, the power α is a function of $p_{\perp}$ and for all particle types grows to be greater than 1.0 at large $p_{\perp}$,[5,9] implying that more than one nucleon is involved. This work has been verified by other experiments,[17,18] and similar behavior has been observed for dihadron systems.[18]

Among the possible explanations of these effects are a change in the single nucleon "sea,"[19] a change in the c.m. energy due to hitting a "tube" of nucleons (coherent tube model[20]), and multiple scattering of bare quarks in the nucleus.[21] So far however, it has been a field in which experiment leads theory.

The data we present here on the power law dependence in A of the cross sections taken with the thin nuclear targets, agree well with our own previously published data. These new data, however, include data on a deuterium target, which increase the lever arm in A and thus improve the accuracy in α. The hydrogen points have not been included in the fits since the π^+ points clearly lie above and the π^- points lie below the extrapolation to A=1.

The invariant cross sections per nucleus for the production of π^+ (upper lines) and π^- (lower lines) are presented in Table IX for Be, Ti, and W targets. Due to limitations on data taking time at 200 and 300 GeV/c, we were not able to take as many data points as at 400 GeV/c.

Figure 12 shows a typical log-log plot of the cross sections for π^- production per nucleus, normalized to a W nucleus, versus atomic weight. One can see that the four complex nuclei are fit very well by the power law form A^{α}; the point for hydrogen (a nucleus with no neutron content) does not lie on the fitted line. The values of α versus $p_{\perp}$ for π^+ and π^- are presented in Table X, and are shown in Fig. 13.

The particle ratios p/π and K/π for these three nuclear targets are presented in Table XI and Table XII, respectively. As an example, Fig. 14 shows the $\bar{p}/\pi^-$ ratio as a function of $p_\perp$ for the H_2, Be, and W targets. The particle ratios K^+/π^+, K^-/π^-, p/π^+, and $\bar{p}/\pi^-$ also show a strong power law A dependence. These ratios for the four nuclear targets at $p_\perp$=3.85 GeV/c are shown in Fig. 15. The exponent in the power law behavior of the K^+/π^+ ratio, for instance is the difference $\alpha_{K^+}(p_\perp)-\alpha_{\pi^+}(p_\perp)$. As examples, the values of the $\alpha_{K^-}\alpha_{\pi}$ differences at 400 GeV/c and the $\alpha_{p-}\alpha_{\pi}$ differences at 300 GeV/c are shown in Figs. 16 and 17, respectively. These differences are presented in Table X. The value of $\alpha_{K^+}-\alpha_{\pi^+}$ is consistent with being flat at large $p_\perp$, but the other particle types show a much stronger A dependence than that for pions at large $p_\perp$. The values for α_{π^+}, α_{π^-}, α_{K^+}, α_{K^-}, α_p, and $\alpha_{\bar{p}}$ are shown in Fig. 18.

Little energy dependence in α is seen. In Fig. 19 the value for α for each particle type is plotted versus beam energy for three values of $p_\perp$; 0.77 GeV/c, 3.08 GeV/c, and 4.62 GeV/c.

In the analysis of Ref 5, lacking hydrogen data we extrapolated the nuclear target data to A=1. These extrapolations were then used to extract the energy dependence parameter n in the expression for the cross section $Ed^3\sigma/d^3p = \frac{1}{p_\perp^n} f(x_\perp)$. For π^- production a value of n = 10.8 ± 0.4 was found, in disagreement with the value of n = 8.5±.5 reported here using the hydrogen target. If we now extrapolate the above nuclear data to A=1 in the same way as in Ref. 5, we find n = 8.7±0.5, in agreement with the hydrogen data.

Extensive reanalysis of our previous results indicates that the most likely reason for the discrepancy was an error in the relative normalization of the runs at the three different energies (a 20% error in the normalization between the 200 and 400 GeV data would account for the discrepancy). In the present data the relative normalization is much more reliable for the following reasons: (1) the transverse dimensions of the targets were large compared to the beam size so that all the beam monitored by the secondary emission monitor strikes the target. (2) The targets were thin so that all the produced particles exited from the downstream face of the target. (3) The data at 200 and 300 GeV were taken simultaneously, the Fermilab accelerator delivering both 200 and 300 GeV protons during the same acceleration cycle.

VI. CONCLUSIONS

We have measured the invariant cross sections at $\theta_{cm} \simeq 90°$ for the production of π^+, π^-, K^+, K^-, p and $\bar{p}$'s for $0.77 \leq p_\perp \leq 6.9$ GeV/c. The incident beam was 200, 300, and 400 GeV protons incident on H_2, D_2, Be, Ti and W targets. The main conclusions are:

1. The invariant cross sections in p-p collisions scale versus $x_\perp$ for $x_\perp > .35$, and are fit well by the form $\frac{1}{p_\perp^n}(1-x_\perp)^b$. The values of n and b are in good agreement with the predictions of the CIM model.[2] In particular the value of n for proton production is different from that for the other particles.

2. The ratio of π^+ to π^- produced in p-p collisions is observed to grow to be much larger than one at large $x_\perp$, and is observed to scale with energy. It agrees with QCD predictions of Feynman, Field and Fox.[13] Proton-neutron cross sections for the production of the above charged hadrons have been derived from p-d and p-p data, and the π^+/π^- ratio is close to one as expected.

3. Data from deuterium, beryllium, titanium, and tungsten targets confirm and extend our previous measurements of the atomic weight dependence.

ACKNOWLEDGMENTS

Many people contributed to the successful operation of this experiment. The staff of the proton laboratory gave much continuing support; we are especially grateful to M. Solis, R. Currier, M. Binkley, T. Murphy. For the cryogenic target and its support we thank M. Otavka, J. Peifer and R. Fast of the Hydrogen Target Group. For engineering support we are indebted to S. Lucero and R. Armstrong at the University of Chicago and to K. Wright at Princeton University. During the data taking phase we were aided by N. Giokaris and J. M. Green (University of Chicago) and J. Mueller (Princeton). C. Whitmer (University of Chicago) was indispensable during the analysis of the data. We would also like to thank the many others at these institutions who gave their support to this work.

REFERENCES

* Research supported by the National Science Foundation and the U. S. Department of Energy.

† Present address: High Energy Physics Laboratory, Harvard University, Cambridge, MA 02138.

†† Permanent address: Ecole Polytechnique, Palaiseau, France.

[1] See, for example, R. F. Cahalan, K. A. Gar, J. Kogut, and L. Susskind, Phys. Rev. D 11, 1199 (1975); B. L. Combridge, J. Kripfganz, and J. Ranft, Phys. Lett. 70B, 234 (1977); R. Cutler and D. Sivers, Phys. Rev. D 16, 679 (1977) and D 17, 196 (1978); A. P. Contogouris, R. Gaskell, and S. Papadopoulos, McGill Univ. Preprint; R. D. Field, Phys. Rev. Lett. 40, 997 (1978); J. F. Gunion UCD Preprint, The Interrelationship of the Constituent Interchange Model and Quantum Chromodynamics; and D. Jones and J. F. Gunion, SLAC-PUB in preparation.

[2] For two good examples among many, see S. J. Brodsky, SLAC-PUB-2009, and R. Blankenbecler, S. J. Brodsky and J. F. Gunion, SLAC-PUB-2057.

[3] R. D. Field and R. P. Feynman, Phys. Rev. D 15, 2590 (1977); R. P. Feynman, R. D. Field, and G. C. Fox, Nucl. Phys. B128, 1 (1977).

[4] M. Banner et al. (SS Collaboration) Phys. Lett. 44B, 537 (1973); F. W. Büsser et al., (CCR Collaboration) Phys. Lett. 46B, 471 (1973); B. Alper et al., (BS Collaboration) Phys. Lett. 44B, 521 and 527 (1973).

[5] J. W. Cronin et al., Phys. Rev. D 11, 3105 (1975).

[6] J. W. Cronin et al., Phys. Rev. Lett. 31, 1426 (1973); D. C. Carey et al., Phys. Rev. Lett. 32, 24 (1974); J. A. Appel et al., Phys. Rev. Lett. 33, 719 (1974); and G. Donaldson et al. (BNL-CIT-LBL Collaboration) Phys. Rev. Lett. 36, 1110 (1976).

[7] D. Antreasyan et al., Phys. Rev. Lett. 38, 112 (1977).

[8] D. Antreasyan et al., Phys. Rev. Lett. 38, 115 (1977).

[9] L. Kluberg et al., Phys. Rev. Lett. 38, 670 (1977).

[10] S. Berman, J. D. Bjorken, and J. Kogut, Phys. Rev. D 4, 3388 (1971); and M. B. Kislinger and S. Ellis, Phys. Rev. D 9, 2027 (1974).

[11] See, for example, Table III of J. F. Gunion's UCD Preprint (Ref. #[1]).

[12] A. P. Clark et al., CERN Preprint (unnumbered).

[13] R. P. Feynman, R. D. Field, G. Fox, CALT 68-651.

[14] S. P. Denisov et al., Nucl. Phys. B61, B62 (1973).

[15] B. Alper et al., Nucl. Phys. B100, 237 (1975).

[16] S. Brodsky and G. Farrar, Phys. Rev. Lett. 31, 1153 (1973); and V. A. Matveev, R. M. Muradyan and A. N. Tavkhelidze, Lett. Nuovo Cimento 7, 719 (1973).

[17] V. Becker et al., Phys. Rev. Lett. 37, 1731 (1976); D. A. Garbutt et al., Phys. Lett. 67B, 355 (1977).

[18] R. L. McCarthy et al., Phys. Rev. Lett. 40, 984 (1978).

[19] A. Krzywicki, Phys. Rev. D 14, 152 (1976).

[20] See, for example, S. Fredriksson, Nucl. Phys. B111, 167 (1976); G. Berlad, A. Dar, and G. Eilam, Phys. Rev. D 13, 161 (1976).

[21] J. H. Kühn, Phys. Rev. D 11, 2948 (1976).

[22] F. W. Büsser et al., Phys. Lett. 55B, 232 (1975).

[23] K. Eggert et al., Nucl. Phys. B 98, 49 (1975).

TABLE CAPTIONS

Table I — The invariant cross sections $Ed^3\sigma/d^3p$ (cm^2 Gev^{-2}) for π^+ (upper lines) and π^- (lower lines) production in 200, 300, and 300 GeV p-p and 400 GeV p-d collisions.

Table II — Experimental values for n, the exponent of the $p_\perp$ in the parametrization $Ed^3\sigma/d^3p = \frac{1}{p_\perp^n} f(x_\perp)$.

Table III — The ratio of π^+ to π^- production versus $p_\perp$ at 200, 300, and 400 GeV in p-p collisions and at 400 GeV in p-d and p-"n" collisions.

Table IV — The production ratio p/π^+ (upper lines) and $\bar{p}/\pi^-$ (lower lines) for 200, 300, and 400 GeV p-p collisions and 400 GeV p-d collisions.

Table V — The production ratio K^+/π^+ (upper lines) and K^-/π^- (lower lines) for 200, 300, and 400 GeV p-p collisions and 400 GeV p-d collisions.

Table VI — The best fit parameters n and b in the parametrization of the form $\frac{1}{p_\perp^n}(1-x_\perp)^b$ for the particle ratios p/π^+, $\bar{p}/\pi^-$, K^+/π^+, and K^-/π^- in p-p collisions.

Table VII — The invariant cross sections $Ed^3\sigma/d^3p$ (cm^2 Gev^{-2}) for K^+ (upper lines) and K^- (lower lines) production in 200, 300, and 400 GeV p-p and 400 GeV p-d collisions.

Table VIII The invariant cross sections $Ed^3\sigma/d^3p$ (cm^2 GeV^{-2}) for p (upper line) and $\bar{p}$ (lower line) production in 200, 300 and 400 GeV p-p and 400 GeV p-d collisions.

Table IX The invariant cross section $Ed^3\sigma/d^3p$ per nucleus (cm^2 GeV^{-2}) for π^+ (upper line) and π^- (lower line) production on Be, Ti, and W targets at 200, 300, and 400 GeV.

Table X The values of the power α_π found in fits to the atomic weight behavior $A^{\alpha(p_\perp)}$ for $\pi^\pm$ and the values of the differences $\alpha_K - \alpha_\pi$, $\alpha_p - \alpha_\pi$ production from D_2, Be, Ti and W targets. The upper line of each $p_\perp$ value is for positive particles; the lower line for negative particles.

Table XI The particle ratios p/π^+ (upper line) and $\bar{p}/\pi^-$ (lower line) for Be, Ti, and W targets.

Table XII The particle ratios K^+/π^+ (upper line) and K^-/π^- (lower line) for Be, Ti, and W targets.

FIGURE CAPTIONS

FIG. 1. The spectrometer.

FIG. 2. The invariant cross section $Ed^3\sigma/d^3p$ for the production of π^- versus $p_\perp$ for 200, 300 and 400 GeV proton-proton collisions.

FIG. 3. The scaling properties of the π^+ and π^- cross sections versus $x_\perp = 2p_\perp/\sqrt{s}$. The cross sections have been multiplied by $p_\perp^n$, where n is the best fit value. The solid line is the fitted parametrization. The fit is over the region $x_\perp > .35$.

FIG. 4. A global plot of lines of constant cross section derived from ISR and Fermilab high energy data on π° and $(\pi^+ + \pi^-)/2$ cross sections near 90°. The solid lines approximate the fits to our data, and have n = 8.4 and b = 9.45. The dashed lines are the fit of Ref. 12.

FIG. 5. The ratio of π^+ to π^- production versus $x_\perp$ for 200, 300, and 400 GeV incident protons. The left hand plot is for p-p collisions; the right hand for p-"n" collisions. The dashed line is the Feynman-Field-Fox QCD prediction of Ref. 13 for $\sqrt{s}$ = 19.4 GeV/c^2.

FIG. 6. The particle ratios p/π and K/π versus $p_\perp$ for 200, 300 and 400 GeV p-p collisions.

FIG. 7. A comparison of the K^+/π^+ ratio versus $p_\perp$ with the B-S Collaboration (Ref. 15) at $\sqrt{s}$ = 23.4 GeV/c^2.

FIG. 8. A comparison of the K^-/π^- ratio versus $p_\perp$ with the B-S Collaboration (Ref. 15) at $\sqrt{s}$ = 23.4 GeV/c^2.

FIG. 9. A comparison of the p/π^+ ratio versus $p_\perp$ with the B-S Collaboration (Ref. 15) at $\sqrt{s}$ = 23.4 GeV/c^2.

FIG. 10. A comparison of the $\bar{p}/\pi^-$ ratio versus $p_\perp$ with the B-S Collaboration (Ref. 15) at $\sqrt{s}$ = 23.4 GeV/c^2.

FIG. 11. The scaling properties of the K/π and p/π particle production ratios in 200, 300, and 400 GeV p-p collisions. The solid line indicates the best fit for $x_\perp \geq 0.35$.

FIG. 12. A plot of the ratio of the cross section for the production of π^- per nucleus for H_2, D_2, Be, Ti, and W targets, normalized to the W yield, plotted versus the atomic weight. The solid line is the power law fit of the form $A^{\alpha(p_\perp)}$. The fit is only to the four complex nucleus data points.

FIG. 13. The value of the power α in the fit A^α versus $p_\perp$ for π^+ and π^- production on D_2, Be, Ti, and W nuclei at $\sqrt{s}$ = 27.4 GeV. The lines, which are identical for π^+ and π^-, are drawn to guide the eye.

FIG. 14. The p/π^+ and $\bar{p}/\pi^-$ ratios as a function of $p_\perp$ for p-p, p-Be, and p-W targets. One can see the strong A dependence at large $p_\perp$.

FIG. 15. A plot of the particle ratios versus atomic weight A at a $p_\perp$ of 3.85 GeV/c. The lines are fits of the form $A^{\Delta\alpha(p_\perp)}$.

FIG. 16. The value of the differences $\alpha_K - \alpha_\pi$ derived from the particle ratios versus $p_\perp$ at 400 GeV/c. The lines are drawn to guide the eye.

FIG. 17. The value of the differences $\alpha_p - \alpha_\pi$ derived from the particle ratios versus $p_\perp$ at 300 GeV/c. The lines are drawn to guide the eye.

FIG. 18. The power α of the A dependence of the invariant cross section versus $p_\perp$ for the production of hadrons by 400 GeV protons; (a) π^+, (b) π^-, (c) K^+, (d) K^-, (e) p, and (f) $\bar{p}$. Unless indicated, the errors are smaller than or equal to the size of the points.

FIG. 19. The energy dependence of the power α of the A dependence of the invariant cross section for the production of hadrons by protons. The points with open circles are for $p_\perp$ = 0.77 GeV/c, with closed circles for $p_\perp$ = 3.08 GeV/c, and open squares for $p_\perp$ = 4.62 GeV/c; (a) π^+, (b) π^-, (c) K^+, (d) K^-, (e) p, (f) $\bar{p}$. Unless indicated, the errors are smaller than or equal to the size of the points.

TABLE I

$p_\perp$ (GeV/c)	p-p			p-d
	200 GeV	300 GeV	400 GeV	400 GeV
0.77	1.02 ± 0.10 1.06 ± 0.11 $\times 10^{-27}$	1.37 ± 0.14 1.22 ± 0.12 $\times 10^{-27}$	1.32 ± 0.13 1.09 ± 0.11 $\times 10^{-27}$	2.75 ± 0.27 2.65 ± 0.27 $\times 10^{-27}$
1.16			1.63 ± 0.16 1.69 ± 0.17 $\times 10^{-28}$	3.43 ± 0.34 3.29 ± 0.33 $\times 10^{-28}$
1.54	1.84 ± 0.09 1.40 ± 0.07 $\times 10^{-29}$	2.44 ± 0.12 2.04 ± 0.10 $\times 10^{-29}$	2.63 ± 0.13 2.31 ± 0.12 $\times 10^{-29}$	5.70 ± 0.28 5.06 ± 0.25 $\times 10^{-29}$
2.31			11.00 ± 0.55 8.88 ± 0.44 $\times 10^{-31}$	2.28 ± 0.11 2.04 ± 0.10 $\times 10^{-30}$
3.08	2.16 ± 0.11 1.68 ± 0.08 $\times 10^{-32}$	4.47 ± 0.22 3.42 ± 0.17 $\times 10^{-32}$	7.04 ± 0.35 5.26 ± 0.26 $\times 10^{-32}$	1.35 ± 0.07 1.16 ± 0.06 $\times 10^{-31}$
3.85			4.52 ± 0.45 3.36 ± 0.17 $\times 10^{-33}$	8.99 ± 0.45 7.60 ± 0.38 $\times 10^{-33}$
4.61	5.89 ± 0.29 2.98 ± 0.15 $\times 10^{-35}$	2.63 ± 0.13 1.44 ± 0.07 $\times 10^{-34}$	4.88 ± 0.24 3.21 ± 0.16 $\times 10^{-34}$	9.28 ± 0.46 7.30 ± 0.37 $\times 10^{-34}$
5.38	4.11 ± 0.41 1.64 ± 0.20 $\times 10^{-36}$	2.80 ± 0.16 1.36 ± 0.08 $\times 10^{-35}$	5.99 ± 0.30 3.48 ± 0.17 $\times 10^{-35}$	10.37 ± 0.52 8.74 ± 0.44 $\times 10^{-35}$
6.15	28.8 ± 6.1 8.1 ± 1.9 $\times 10^{-38}$	2.36 ± 0.21 1.14 ± 0.09 $\times 10^{-36}$	9.63 ± 0.57 4.29 ± 0.25 $\times 10^{-36}$	1.65 ± 0.10 1.26 ± 0.07 $\times 10^{-35}$
6.91			15.2 ± 2.0 6.1 ± 1.0 $\times 10^{-37}$	2.48 ± 0.29 1.76 ± 0.27 $\times 10^{-36}$

TABLE II

Group	Ref.	Particle	n
CCR	4	π°	8.24 ± .7
CCRS	22	π°	8.6 ± .1
		π^+	7.5 ± .2
		π^-	7.9 ± .3
B-S	15	$\pi^\pm$	Consistent with n = 8
ACHM	23	π°	7.2 ± .2
BNL-CIT-LBL	6	π°	10.8 ± .4
CSE	12	π°	6.6 ± 0.8
This experiment		π^+	8.2 ± .5
		π^-	8.5 ± .5

TABLE III

	p-p			p-d	p-"n"
$p_\perp$(GeV/c)	200 GeV	300 Gev	400 GeV	400 GeV	400 GeV
0.77	0.96±0.10	1.12±0.11	1.21±0.12	1.04±0.10	0.92±0.09
1.16	- -	- -	0.97±0.10	1.05±0.10	1.13±0.11
1.54	1.31±0.13	1.20±0.12	1.14±0.11	1.13±0.11	1.12±0.11
2.31	- -	- -	1.24±0.12	1.12±0.11	1.02±0.10
3.08	1.29±0.13	1.31±0.13	1.34±0.13	1.16±0.12	1.02±0.10
3.85	- -	- -	1.34±0.13	1.18±0.12	1.06±0.11
4.61	1.98±0.20	1.83±0.18	1.52±0.15	1.27±0.13	1.08±0.11
5.30	2.51±0.40	2.06±0.21	1.72±0.17	1.19±0.12	0.83±0.10
6.15	3.55±1.12	2.07±0.23	2.24±0.22	1.31±0.13	0.82±0.16
6.91	- -	- -	2.49±0.51	1.41±0.27	0.84±0.37

TABLE IV

$p_\perp$ (GeV/c)	p-p			p-d
	200 GeV	300 GeV	400 GeV	400 GeV
0.77	0.25 ± 0.01 0.059 ± 0.003	0.21 ± 0.01 0.066 ± 0.002	0.21 ± 0.01 0.070 ± 0.003	0.21 ± 0.01 0.075 ± 0.003
1.16		0.36 ± 0.01 0.100 ± 0.002	0.34 ± 0.01 0.106 ± 0.004	0.37 ± 0.01 0.116 ± 0.004
1.54	0.54 ± 0.02 0.095 ± 0.003	0.46 ± 0.01 0.103 ± 0.002	0.43 ± 0.01 0.114 ± 0.002	0.46 ± 0.01 0.120 ± 0.003
2.31		0.52 ± 0.01 0.092 ± 0.003	0.47 ± 0.01 0.099 ± 0.004	0.52 ± 0.01 0.091 ± 0.005
3.08	0.60 ± 0.01 0.050 ± 0.002	0.47 ± 0.01 0.064 ± 0.002	0.42 ± 0.01 0.067 ± 0.002	0.45 ± 0.01 0.071 ± 0.002
3.85		0.39 ± 0.01 0.033 ± 0.003	0.33 ± 0.01 0.041 ± 0.002	0.36 ± 0.01 0.041 ± 0.002
4.61	0.41 ± 0.04 0.010 ± 0.004	0.30 ± 0.01 0.020 ± 0.003	0.27 ± 0.01 0.021 ± 0.003	0.26 ± 0.02 0.023 ± 0.003
5.38	0.27 ± 0.07 0.028 ± 0.020	0.20 ± 0.02 0.008 ± 0.004	0.20 ± 0.01 0.017 ± 0.004	0.24 ± 0.02 0.011 ± 0.004
6.15	0.37 ± 0.13	0.17 ± 0.03 0.008 ± 0.006	0.12 ± 0.02 0.019 ± 0.007	0.14 ± 0.03 0.003 ± 0.003
6.91		0.14 ± 0.05	0.08 ± 0.02	0.13 ± 0.06

TABLE V

$p_\perp$ (GeV/c)	p-p			p-d
	200 GeV	300 GeV	400 GeV	400 GeV
0.77	0.21 ± 0.02 0.15 ± 0.02	0.19 ± 0.02 0.16 ± 0.02	0.21 ± 0.03 0.17 ± 0.02	0.19 ± 0.02 0.14 ± 0.02
1.16		0.28 ± 0.02 0.20 ± 0.02	0.30 ± 0.03 0.21 ± 0.02	0.31 ± 0.03 0.20 ± 0.02
1.54	0.32 ± 0.02 0.20 ± 0.01	0.33 ± 0.02 0.22 ± 0.01	0.36 ± 0.03 0.25 ± 0.02	0.34 ± 0.03 0.23 ± 0.02
2.31		0.39 ± 0.02 0.25 ± 0.01	0.41 ± 0.03 0.27 ± 0.02	0.44 ± 0.03 0.25 ± 0.02
3.08	0.42 ± 0.02 0.20 ± 0.01	0.45 ± 0.01 0.25 ± 0.01	0.46 ± 0.03 0.27 ± 0.02	0.46 ± 0.03 0.24 ± 0.02
3.85		0.46 ± 0.02 0.22 ± 0.01	0.47 ± 0.03 0.24 ± 0.01	0.47 ± 0.03 0.20 ± 0.01
4.61	0.51 ± 0.04 0.13 ± 0.02	0.42 ± 0.02 0.15 ± 0.01	0.46 ± 0.03 0.19 ± 0.01	0.49 ± 0.04 0.15 ± 0.01
5.38	0.55 ± 0.08 0.06 ± 0.03	0.38 ± 0.02 0.11 ± 0.01	0.40 ± 0.02 0.13 ± 0.01	0.49 ± 0.05 0.09 ± 0.01
6.15	0.36 ± 0.11	0.50 ± 0.05 0.08 ± 0.02	0.45 ± 0.03 0.06 ± 0.01	0.44 ± 0.06 0.06 ± 0.02
6.91		0.58 ± 0.11 0.04 ± 0.04	0.53 ± 0.08 0.09 ± 0.04	0.35 ± 0.13 0.13 ± 0.06

Table VI

Ratio	n	b	χ^2/DOF
p/π^+	n = 3.62 ± 1.5	b = -1.67 ± 1.0	5.3/7
$\bar{p}/\pi^-$	n = 0.27 ± 1.7	b = 4.29 ± 1.9	3.1/4
K^+/π^+	n = 0.20 ± 0.5	b = -0.68 ± 0.4	15.1/7
K^-/π^-	n = 1.58 ± 1.4	b = 1.59 ± 1.2	9.0/6

TABLE VII

$p_\perp$ (GeV/c)	p-p			p-d
	200 GeV	300 GeV	400 GeV	400 GeV
0.77	2.1 ±0.3 1.6 ±0.2 x10^{-28}	2.6 ±0.4 2.0 ±0.3 x10^{-28}	2.8 ±0.5 1.9 ±0.3 x10^{-28}	5.2 ±0.8 3.7 ±0.7 x10^{-28}
1.16	- - - -	- - - -	4.9 ±0.7 3.5 ±0.5 x10^{-29}	1.1 ±0.1 0.66±0.09 x10^{-28}
1.54	5.9 ±0.4 2.8 ±0.2 x10^{-30}	8.1 ±0.6 4.5 ±0.3 x10^{-30}	9.4 ±0.9 5.8 ±0.5 x10^{-30}	1.9 ±0.2 1.2 ±0.1 x10^{-29}
2.31	- - - -	- - - -	4.5 ±0.4 2.4 ±0.2 x10^{-31}	1.0 ±0.1 0.51±0.05 x10^{-30}
3.08	9.1 ±0.6 3.4 ±0.2 x10^{-33}	2.0 ±0.1 0.86±0.6 x10^{-32}	3.2 ±0.3 1.4 ±0.1 x10^{-32}	6.2 ±0.5 2.8 ±0.3 x10^{-32}
3.85	- - - -	- - - -	2.1 ±0.2 0.81±0.05 x10^{-33}	4.2 ±0.3 1.5 ±0.1 x10^{-33}
4.61	3.0 ±0.3 0.39±0.06 x10^{-35}	1.1 ±0.1 0.22±0.02 x10^{-34}	2.2 ±0.2 0.61±0.04 x10^{-34}	4.5 ±0.4 1.1 ±0.1 x10^{-34}
5.38	2.3 ±0.4 0.10±0.05 x10^{-36}	1.1 ±0.1 0.15±0.02 x10^{-35}	2.4 ±0.2 0.46±0.04 x10^{-35}	5.1 ±0.6 0.79±0.10 x10^{-35}
6.15	1.0 ±0.4 - ± - x10^{-37}	1.2 ±0.2 0.09±0.02 x10^{-36}	4.3 ±0.4 0.26±0.05 x10^{-36}	7.3 ±1.1 0.76±0.26 x10^{-36}
6.91	- - - -	- - - -	8.1 ±1.6 0.55±0.26 x10^{-37}	8.7 ±3.4 2.3 ±1.1 x10^{-37}

TABLE VIII

$p_\perp$ (GeV/c)	p-p						p-d	
	200 GeV		300 GeV		400 GeV		400 GeV	
0.77	2.6 ±0.3 0.62 ±0.07	$\times 10^{-28}$	2.9 ±0.3 0.80±0.08	$\times 10^{-28}$	2.8 ±0.3 0.76 ±0.08	$\times 10^{-28}$	5.8 ±0.6 2.0 ±0.2	$\times 10^{-28}$
1.16	- - - -		- - - -		5.5 ±0.6 1.8 ±0.2	$\times 10^{-29}$	1.3 ±0.1 0.38 ±0.04	$\times 10^{-28}$
1.54	9.9 ±0.6 1.3 ±0.1	$\times 10^{-30}$	1.12±0.06 0.21±0.01	$\times 10^{-29}$	1.1 ±0.1 0.26 ±0.01	$\times 10^{-29}$	2.6 ±0.1 0.61 ±0.03	$\times 10^{-29}$
2.31	- - - -		- - - -		5.2 ±0.3 0.88 ±0.06	$\times 10^{-31}$	1.2 ±0.1 0.19 ±0.01	$\times 10^{-30}$
3.08	1.30 ±0.07 0.084±0.005	$\times 10^{-32}$	2.1 ±0.1 0.22±0.01	$\times 10^{-32}$	3.0 ±0.2 0.35 ±0.02	$\times 10^{-32}$	6.1 ±0.3 0.82 ±0.05	$\times 10^{-32}$
3.85	- - - -		- - - -		1.5 ±0.2 0.14 ±0.01	$\times 10^{-33}$	3.2 ±0.2 0.31 ±0.02	$\times 10^{-33}$
4.61	2.40 ±0.03 0.030±0.012	$\times 10^{-35}$	7.9 ±0.5 0.29±0.04	$\times 10^{-35}$	1.3 ±0.1 0.067±0.010	$\times 10^{-34}$	2.4 ±0.2 0.17 ±0.02	$\times 10^{-34}$
5.38	1.10 ±0.30 0.046±0.033	$\times 10^{-36}$	5.6 ±0.6 0.11±0.06	$\times 10^{-36}$	1.2 ±0.1 0.059±0.014	$\times 10^{-35}$	2.5 ±0.2 0.096±0.035	$\times 10^{-35}$
6.15	1.1 ±0.4 - ± -	$\times 10^{-37}$	4.0 ±0.8 0.09±0.07	$\times 10^{-37}$	1.2 ±0.2 0.082±0.030	$\times 10^{-36}$	2.3 ±0.5 0.038±0.038	$\times 10^{-36}$
6.91	- - - -		- - - -		1.2 ±0.3 - -	$\times 10^{-37}$	3.2 ±1.5 - -	$\times 10^{-37}$

TABLE IX

$P_\perp$ (GeV/c)	Tungsten (W) Target			Titanium Target			Beryllium Target		
	200 GeV	300 GeV	400 GeV	200 GeV	300 GeV	400 GeV	200 GeV	300 GeV	400 GeV
0.77	1.01±0.10 1.03±0.10 $\times 10^{-25}$	1.41±0.14 1.30±0.13 $\times 10^{-25}$	1.58±0.16 1.60±0.16 $\times 10^{-25}$	3.23±0.32 3.17±0.32 $\times 10^{-26}$	4.28±0.43 4.05±0.41 $\times 10^{-26}$	4.47±0.43 4.57±0.46 $\times 10^{-26}$	8.98±0.90 8.37±0.84 $\times 10^{-27}$	1.07±0.11 1.00±0.10 $\times 10^{-26}$	1.16±0.12 1.09±0.11 $\times 10^{-26}$
1.16	- - - -	- - - -	2.42±0.24 2.40±0.24 $\times 10^{-26}$	- - - -	- - - -	6.46±0.65 6.86±0.69 $\times 10^{-27}$	- - - -	- - - -	1.47±0.15 1.47±0.15 $\times 10^{-27}$
1.54	2.74±0.14 2.31±0.12 $\times 10^{-27}$	3.74±0.19 3.33±0.17 $\times 10^{-27}$	4.68±0.23 4.49±0.22 $\times 10^{-27}$	- - - -	- - - -	1.16±0.85 1.17±0.06 $\times 10^{-27}$	- - - -	- - - -	2.64±0.13 2.43±0.12 $\times 10^{-28}$
2.31	- - - -	- - - -	2.56±0.13 2.34±0.12 $\times 10^{-28}$	- - - -	- - - -	6.21±0.31 5.33±0.27 $\times 10^{-29}$	- - - -	- - - -	1.15±0.06 1.05±0.05 $\times 10^{-29}$
3.08	6.03±0.30 5.12±0.26 $\times 10^{-30}$	1.18±0.06 1.08±0.05 $\times 10^{-29}$	1.86±0.09 1.68±0.08 $\times 10^{-29}$	1.28±0.06 1.08±0.05 $\times 10^{-30}$	2.60±0.13 2.33±0.12 $\times 10^{-30}$	4.02±0.20 3.69±0.18 $\times 10^{-30}$	2.22±0.11 1.94±0.10 10^{-31}	4.36±0.22 3.99±0.20 $\times 10^{-31}$	7.41±0.37 6.23±0.31 $\times 10^{-31}$
3.85	- - - -	- - - -	1.43±0.07 1.30±0.07 $\times 10^{-30}$	- - - -	- - - -	3.14±0.16 2.93±0.15 $\times 10^{-31}$	- - - -	- - - -	5.22±0.26 4.27±0.21 $\times 10^{-32}$
4.61	2.04±0.10 1.52±0.08 $\times 10^{-32}$	7.33±0.37 6.35±0.32 $\times 10^{-32}$	1.35±0.07 1.23±0.06 $\times 10^{-31}$	4.20±0.21 2.89±0.14 $\times 10^{-33}$	1.45±0.07 1.22±0.06 $\times 10^{-32}$	3.11±0.16 2.46±0.12 $\times 10^{-32}$	6.18±0.31 4.43±0.22 $\times 10^{-34}$	2.44±0.12 2.02±0.10 $\times 10^{-33}$	4.26±0.31 3.78±0.19 $\times 10^{-33}$
5.38	13.02±0.95 6.39±0.48 $\times 10^{-34}$	6.60±0.37 5.51±0.28 $\times 10^{-33}$	1.66±0.08 1.36±0.07 $\times 10^{-32}$	- - - -	- - - -	3.19±0.26 2.59±0.14 $\times 10^{-33}$	- - - -	- - - -	5.49±0.32 4.72±0.24 $\times 10^{-34}$
6.15	8.85±1.32 4.54±1.17 $\times 10^{-35}$	7.09±0.53 5.23±0.59 $\times 10^{-34}$	1.91±0.17 1.66±0.00 $\times 10^{-33}$	- - - -	- - - -	3.84±0.62 - - $\times 10^{-34}$	- - - -	- - - -	6.86±1.11 - - $\times 10^{-35}$
6.91	- - - -	- - - -	2.81±0.40 2.31±0.25 $\times 10^{-34}$	- - - -	- - - -	- - - -	- - - -	- - - -	- - - -

TABLE X

$p_\perp$ (GeV/c)	200 GeV			300 GeV			400 GeV		
	α_π	$\alpha_K - \alpha_\pi$	$\alpha_p - \alpha_\pi$	α_π	$\alpha_K - \alpha_\pi$	$\alpha_p - \alpha_\pi$	α_π	$\alpha_K - \alpha_\pi$	$\alpha_p - \alpha_\pi$
0.77	0.810±0.015 0.840±0.016	-0.012±0.029 -0.027±0.015	0.081±0.028 - -	0.860±0.015 0.854±0.015	0.059±0.020 0.040±0.023	0.066±0.014 0.036±0.017	0.904±0.005 0.906±0.005	0.058±0.016 0.073±0.013	0.090±0.014 0.002±0.013
1.16	- - - -	- - - -	- - - -	- - - -	- - - -	- - - -	0.943±0.005 0.943±0.005	0.047±0.009 0.046±0.007	0.075±0.009 0.000±0.009
1.54	- - - -	- - - -	- - - -	- - - -	- - - -	- - - -	0.982±0.007 0.989±0.005	0.035±0.005 0.024±0.005	0.085±0.003 0.052±0.005
2.31	- - - -	- - - -	- - - -	- - - -	- - - -	- - - -	1.046±0.005 1.051±0.005	0.030±0.009 0.019±0.006	0.105±0.004 0.073±0.009
3.08	1.11 ±0.02 1.10 ±0.02	0.018±0.014 0.034±0.014	0.099±0.014 - -	1.10 ±0.02 1.10 ±0.02	0.037±0.014 0.010±0.014	0.110±0.014 0.070±0.014	1.092±0.007 1.100±0.005	0.033±0.005 0.028±0.004	0.137±0.002 0.097±0.006
3.85	- - - -	- - - -	- - - -	- - - -	- - - -	- - - -	1.120±0.006 1.137±0.005	0.035±0.005 0.051±0.007	0.156±0.005 0.151±0.012
4.61	1.16 ±0.02 1.19 ±0.02	0.041±0.029 0.004±0.040	0.152±0.023 - -	1.14 ±0.02 1.16 ±0.02	0.027±0.016 0.076±0.018	0.192±0.020 0.064±0.031	1.109±0.008 1.148±0.010	0.044±0.015 0.079±0.012	0.231±0.013 0.200±0.025
5.38	- - - -	- - - -	- - - -	- - - -	- - - -	- - - -	1.128±0.009 1.129±0.014	0.023±0.014 0.160±0.024	0.199±0.018 0.31 ±0.07
6.15	- - - -	- - - -	- - - -	- - - -	- - - -	- - - -	1.074±0.021 1.082±0.015	0.050±0.032 0.194±0.056	0.248±0.045 0.41 ±0.22
6.91	- - - -	- - - -	- - - -	- - - -	- - - -	- - - -	1.048±0.043 1.085±0.007	0.06 ±0.09 -0.04 ±0.12	0.27 ±0.10 - -

TABLE XI

$P_\perp$ (GeV/c)	W Target			Ti Target			Be Target		
	200 GeV	300 GeV	400 GeV	200 GeV	300 GeV	400 GeV	200 GeV	300 GeV	400 GeV
0.77	0.328±0.011 0.068±0.005	0.304±0.004 0.074±0.002	0.294±0.015 0.068±0.003	0.334±0.008 0.067±0.003	0.289±0.006 0.073±0.003	0.264±0.005 0.071±0.004	0.261±0.006 0.056±0.003	0.250±0.006 0.066±0.003	0.226±0.011 0.065±0.003
1.16	- - - -	0.507±0.005 0.107±0.003	0.487±0.015 0.110±0.003	- - - -	- - - -	0.433±0.013 0.111±0.003	- - - -	- - - -	0.318±0.010 0.115±0.003
1.54	0.797±0.023 0.104±0.007	0.694±0.007 0.123±0.003	0.641±0.005 0.145±0.002	- - - -	- - - -	0.579±0.005 0.138±0.002	- - - -	- - - -	0.497±0.004 0.126±0.002
2.31	- - - -	0.871±0.016 0.118±0.005	0.794±0.008 0.135±0.003	- - - -	- - - -	0.705±0.007 0.131±0.003	- - - -	- - - -	0.581±0.007 0.116±0.003
3.08	1.047±0.014 0.069±0.002	0.857±0.008 0.094±0.001	0.789±0.005 0.109±0.002	0.936±0.011 0.066±0.002	0.737±0.007 0.084±0.003	0.686±0.004 0.099±0.001	0.779±0.010 0.059±0.002	0.615±0.006 0.076±0.002	0.529±0.003 0.085±0.001
3.85	- - - -	0.802±0.009 0.059±0.002	0.712±0.006 0.077±0.002	- - - -	- - - -	0.600±0.012 0.061±0.004	- - - -	- - - -	0.449±0.007 0.049±0.003
4.61	1.026±0.033 0.028±0.003	0.713±0.008 0.044±0.002	0.633±0.015 0.054±0.002	0.76 ±0.04 0.028±0.006	0.606±0.017 0.042±0.004	0.431±0.022 0.046±0.003	0.67 ±0.04 0.030±0.006	0.396±0.015 0.036±0.003	0.339±0.019 0.026±0.004
5.38	0.94 ±0.08 0.017±0.012	0.657±0.022 0.028±0.004	0.510±0.015 0.038±0.004	- - - -	- - - -	0.420±0.04 0.021±0.005	- - - -	- - - -	0.259±0.020 0.015±0.003
6.15	0.81 ±0.15 - -	0.54 ±0.03 0.011±0.010	0.46 ±0.05 0.019±0.004	- - - -	- - - -	0.32 ±0.05 - -	- - - -	- - - -	0.29 ±0.05 - -
6.91	- - - -	0.34 ±0.10 0.02 ±0.02	0.34 ±0.08 0.008±0.008	- - - -	- - - -	- - - -	- - - -	- - - -	- - - -

TABLE XII

$p_\perp$ (GeV/c)	W Target			Ti Target			Be Target		
	200 GeV	300 GeV	400 GeV	200 GeV	300 GeV	400 GeV	200 GeV	300 GeV	400 GeV
0.77	0.226±0.018 0.151±0.015	0.277±0.008 0.195±0.008	0.27 ± 0.03 0.20 ± 0.02	0.240±0.014 0.146±0.010	0.244±0.011 0.184±0.008	0.24 ±0.02 0.17 ±0.02	0.238±0.012 0.159±0.009	0.235±0.012 0.173±0.010	0.24 ±0.02 0.16 ±0.02
1.16	- - - -	0.341±0.007 0.223±0.006	0.374±0.020 0.243±0.013	- - - -	- - - -	0.335±0.18 0.236±0.14	- - - -	- - - -	0.315±0.018 0.203±0.011
1.54	0.386±0.022 0.204±0.013	0.413±0.007 0.239±0.005	0.402±0.021 0.254±0.013	- - - -	- - - -	0.390±0.021 0.255±0.004	- - - -	- - - -	0.369±0.019 0.235±0.012
2.31	- - - -	0.467±0.014 0.266±0.008	0.496±0.026 0.272±0.015	- - - -	- - - -	0.461±0.024 0.275±0.015	- - - -	- - - -	0.444±0.023 0.256±0.014
3.08	0.487±0.010 0.222±0.005	0.525±0.007 0.254±0.003	0.522±0.026 0.274±0.014	0.489±0.009 0.210±0.004	0.488±0.007 0.249±0.005	0.497±0.025 0.263±0.013	0.462±0.029 0.200±0.004	0.469±0.008 0.246±0.005	0.474±0.024 0.254±0.013
3.85	- - - -	0.567±0.008 0.246±0.004	0.557±0.029 0.258±0.014	- - - -	- - - -	0.540±0.030 0.240±0.015	- - - -	- - - -	0.501±0.026 0.222±0.013
4.61	0.585±0.026 0.160±0.009	0.546±0.008 0.203±0.005	0.572±0.033 0.224±0.012	0.518±0.033 0.132±0.014	0.536±0.018 0.202±0.009	0.497±0.037 0.206±0.013	0.53 ±0.04 0.166±0.016	0.502±0.019 0.158±0.008	0.46 ±0.03 0.184±0.014
5.38	0.63 ±0.07 0.12 ±0.03	0.584±0.023 0.152±0.011	0.530±0.031 0.195±0.013	- - - -	- - - -	0.55 ±0.06 0.139±0.015	- - - -	- - - -	0.47 ±0.04 0.129±0.012
6.15	0.68 ±0.14 0.08 ±0.08	0.62 ±0.04 0.13 ±0.03	0.59 ±0.06 0.139±0.012	- - - -	- - - -	0.46 ±0.07 - -	- - - -	- - - -	0.56 ±0.08 - -
6.91	- - - -	0.39 ±0.12 0.06 ±0.04	0.48 ±0.11 0.11 ±0.03	- - - -	- - - -	- - - -	- - - -	- - - -	- - - -

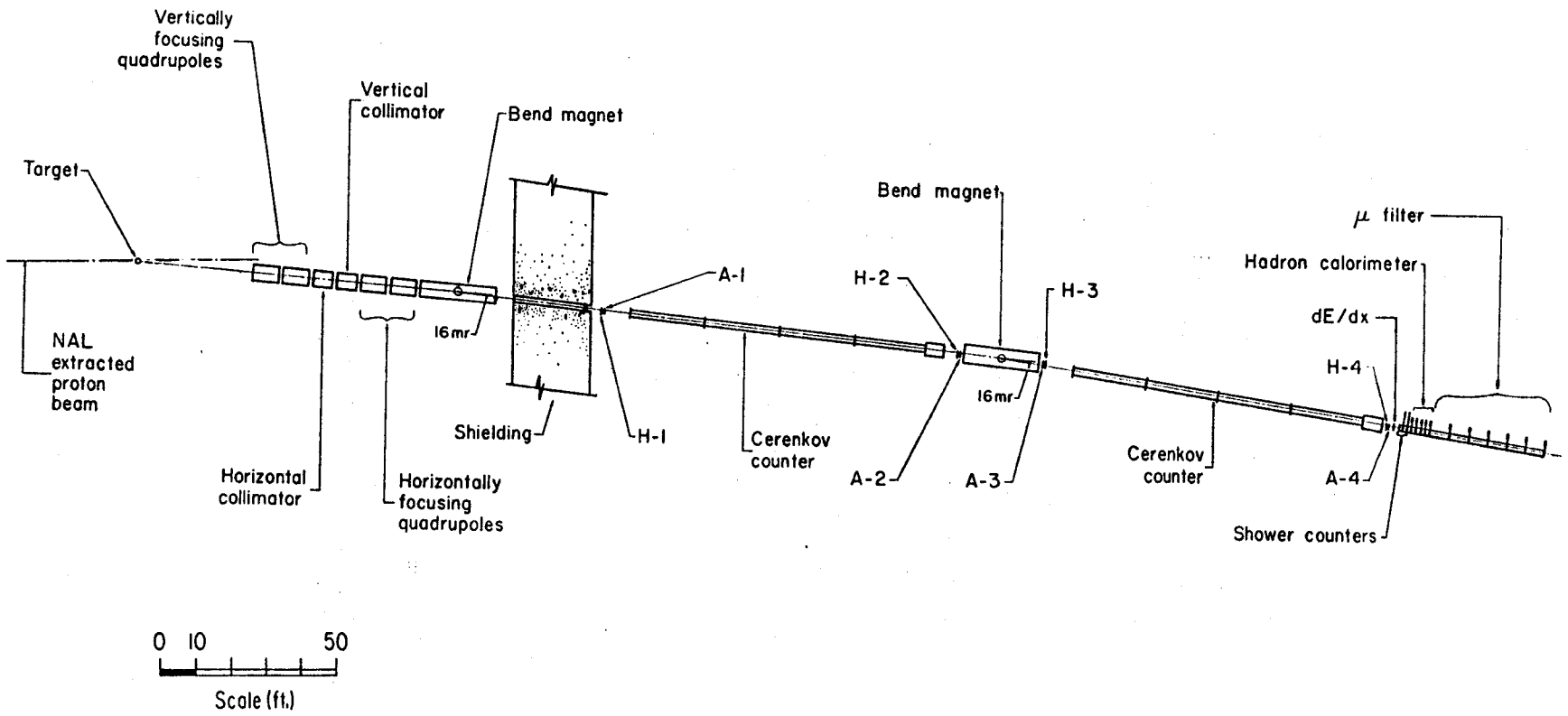
Vertically focusing quadrupoles
Vertical collimator
Bend magnet
Target
Bend magnet
μ filter
Hadron calorimeter
A-1
H-2
H-3
dE/dx
NAL extracted proton beam
16mr
H-4
16mr
Shielding
H-1
Cerenkov counter
A-2
A-3
Cerenkov counter
A-4
Horizontal collimator
Horizontally focusing quadrupoles
Shower counters
0 10 50
Scale (ft.)

FIG. 1.

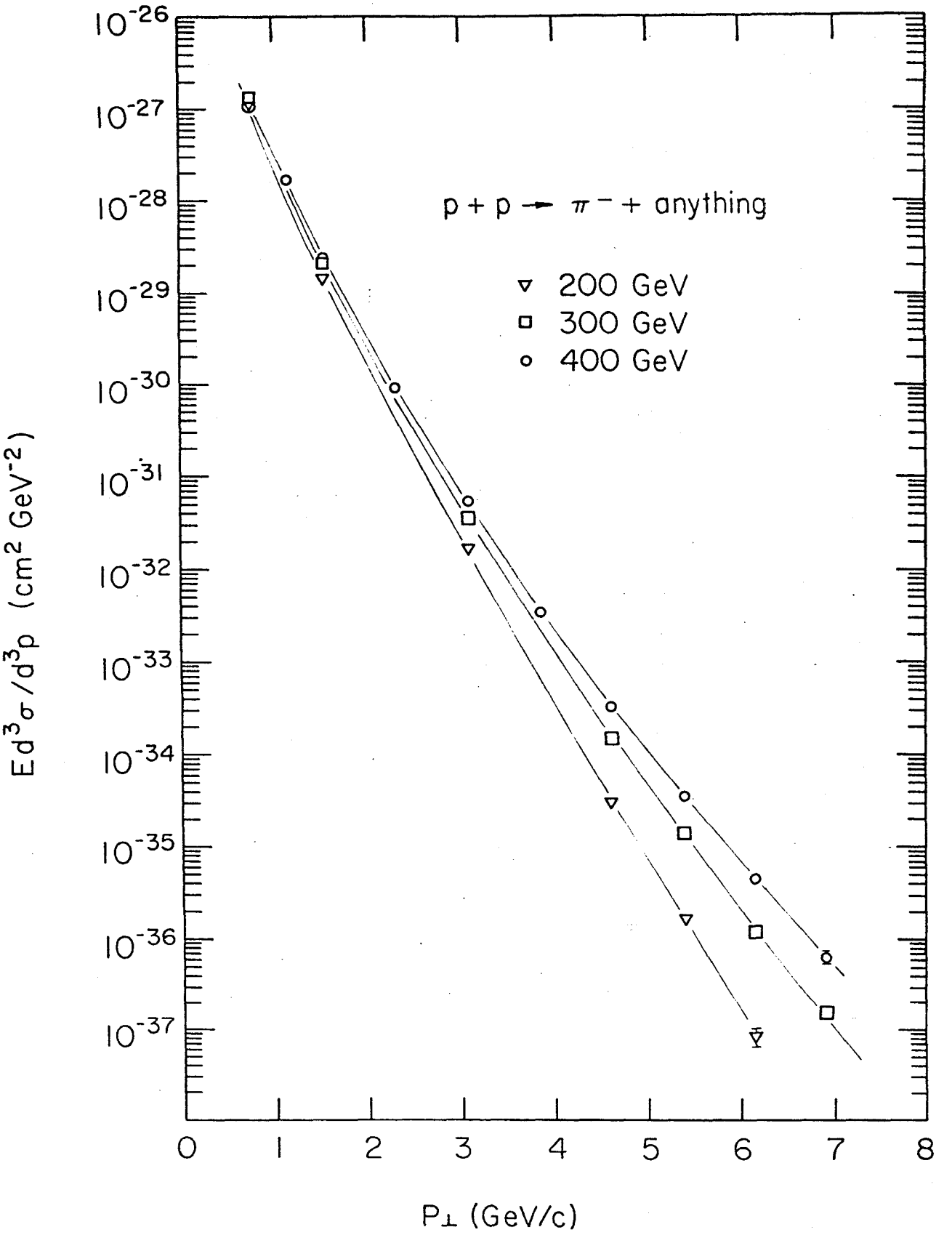
10^{-26}
10^{-27}
10^{-28}
10^{-29}
10^{-30}
10^{-31}
10^{-32}
10^{-33}
10^{-34}
10^{-35}
10^{-36}
10^{-37}
$Ed^3\sigma/d^3p$ (cm^2 GeV^{-2})
$p + p \rightarrow \pi^- +$ anything
200 GeV
300 GeV
400 GeV
0
1
2
3
4
5
6
7
8
$P_\perp$ (GeV/c)

FIG. 2.

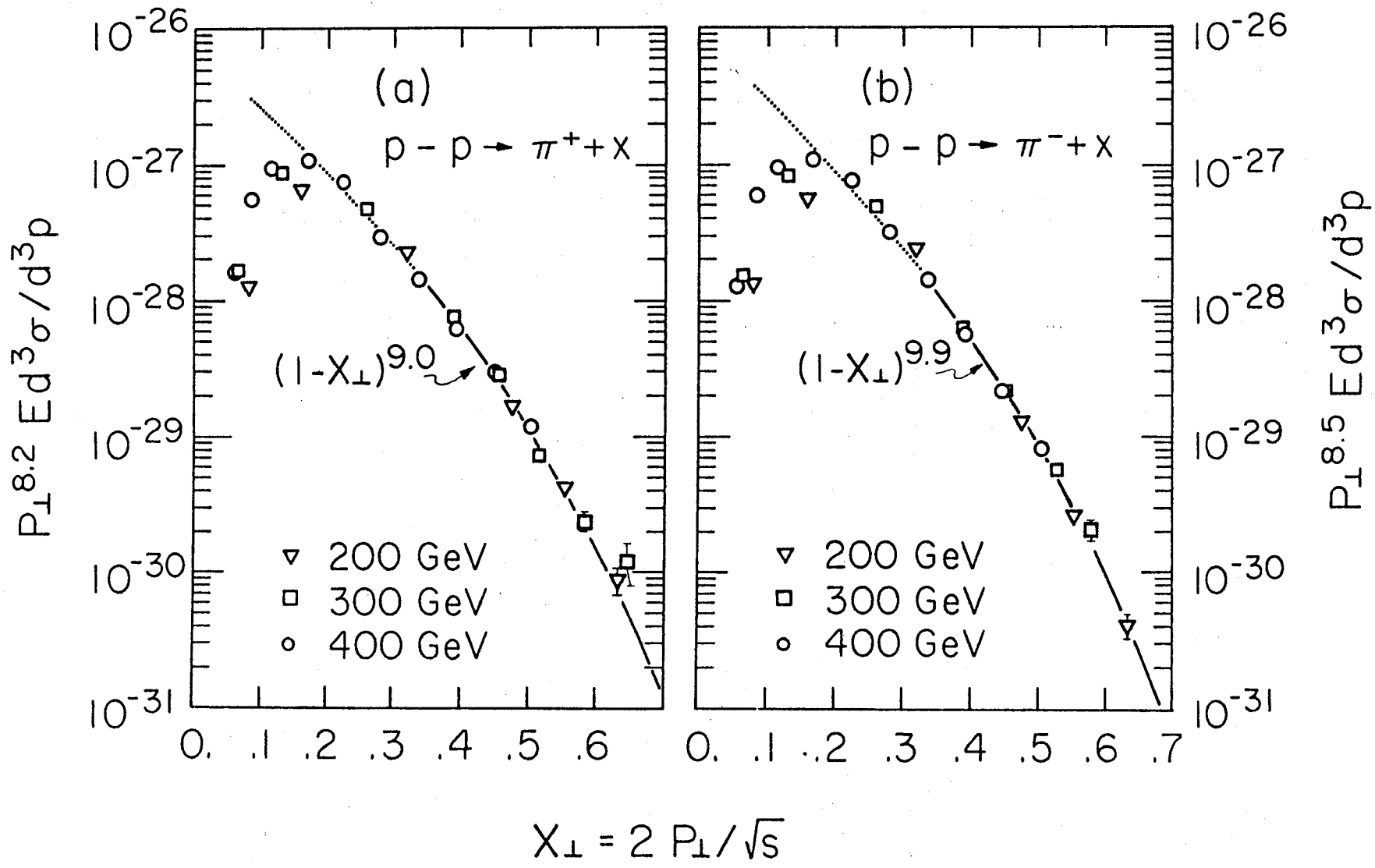
(a)
p - p → π⁺ + X
(1-X⊥)^9.0
200 GeV
300 GeV
400 GeV
(b)
p - p → π⁻ + X
(1-X⊥)^9.9
200 GeV
300 GeV
400 GeV
P⊥^8.2 Ed³σ/d³p
P⊥^8.5 Ed³σ/d³p
X⊥ = 2 P⊥/√s

FIG. 3.

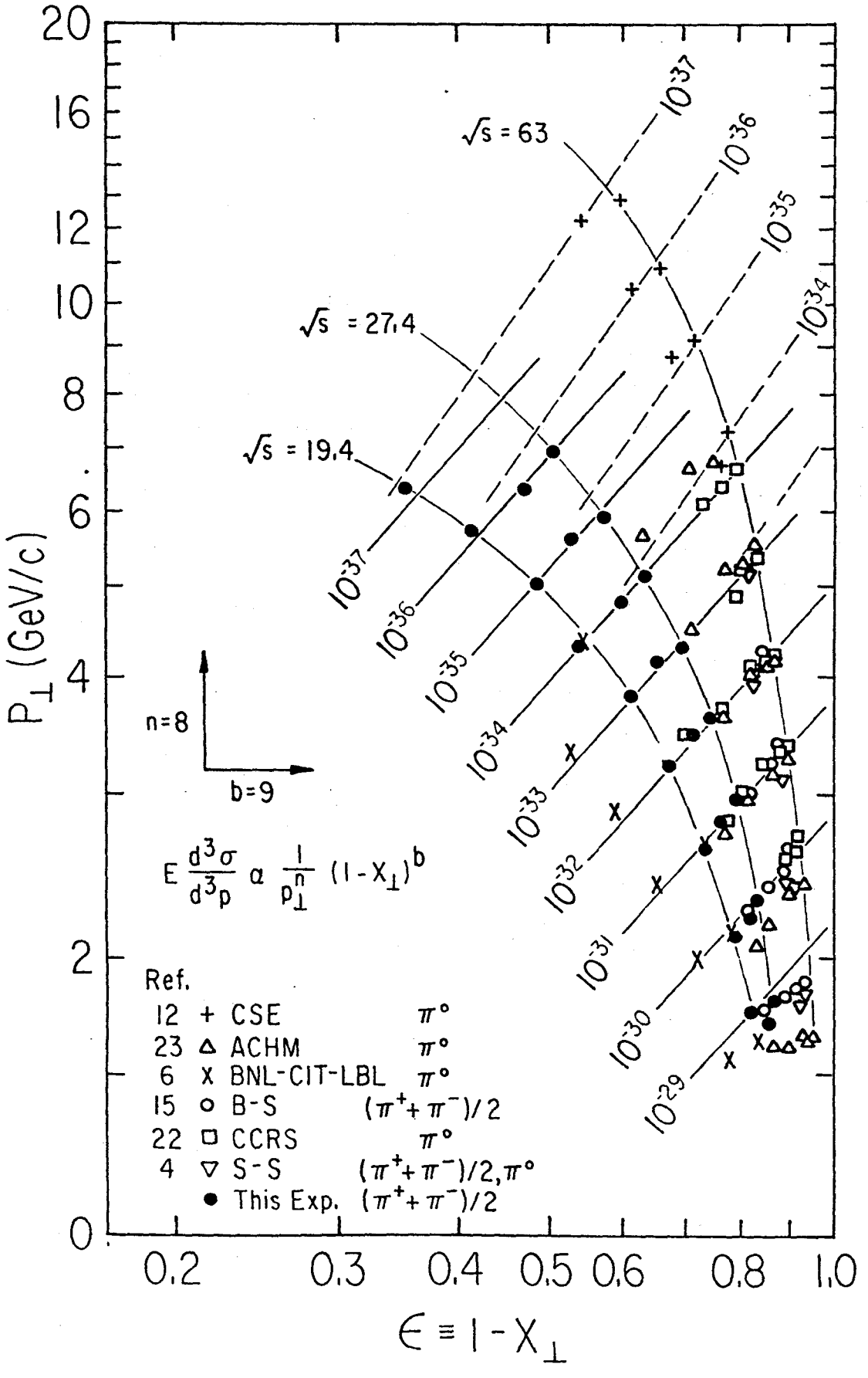
20
16
12
10
8
6
4
2
0
$P_\perp$ (GeV/c)
0.2
0.3
0.4
0.5
0.6
0.8
1.0
$\epsilon \equiv 1 - X_\perp$
$\sqrt{s}$ = 63
$\sqrt{s}$ = 27.4
$\sqrt{s}$ = 19.4
10^{-37}
10^{-36}
10^{-35}
10^{-34}
10^{-33}
10^{-32}
10^{-31}
10^{-30}
10^{-29}
n=8
b=9
$E\frac{d^3\sigma}{d^3p} \alpha \frac{1}{p_\perp^n}(1-X_\perp)^b$
Ref.
12 + CSE π°
23 Δ ACHM π°
6 X BNL-CIT-LBL π°
15 o B-S $(\pi^+ + \pi^-)/2$
22 □ CCRS π°
4 ▽ S-S $(\pi^+ + \pi^-)/2, \pi^\circ$
● This Exp. $(\pi^+ + \pi^-)/2$

FIG. 4.

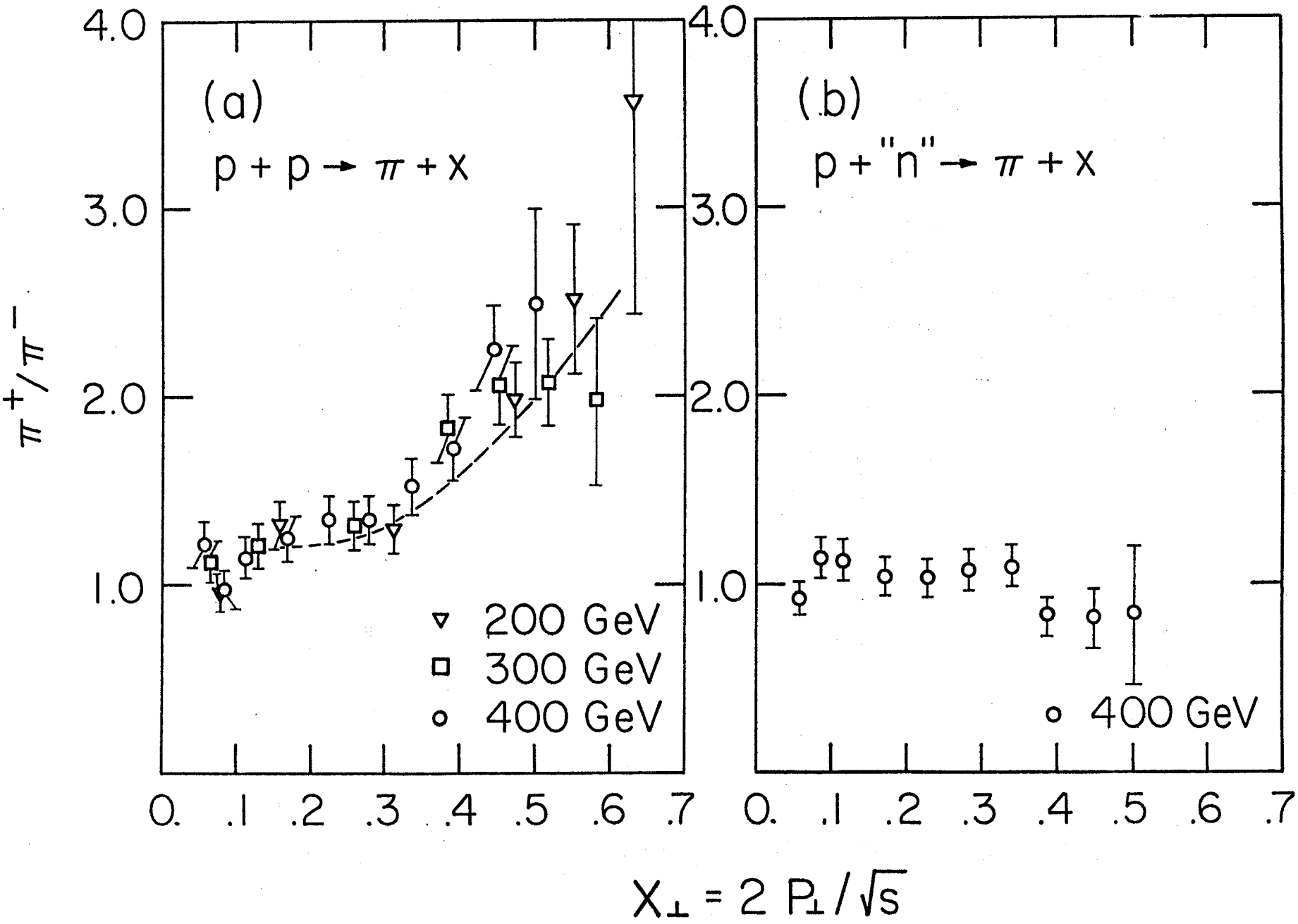
(a)
p + p → π + X
(b)
p + "n" → π + X
200 GeV
300 GeV
400 GeV
400 GeV
π+/π−
4.0
3.0
2.0
1.0
0.
.1
.2
.3
.4
.5
.6
.7
X⊥ = 2 P⊥/√s

FIG. 5.

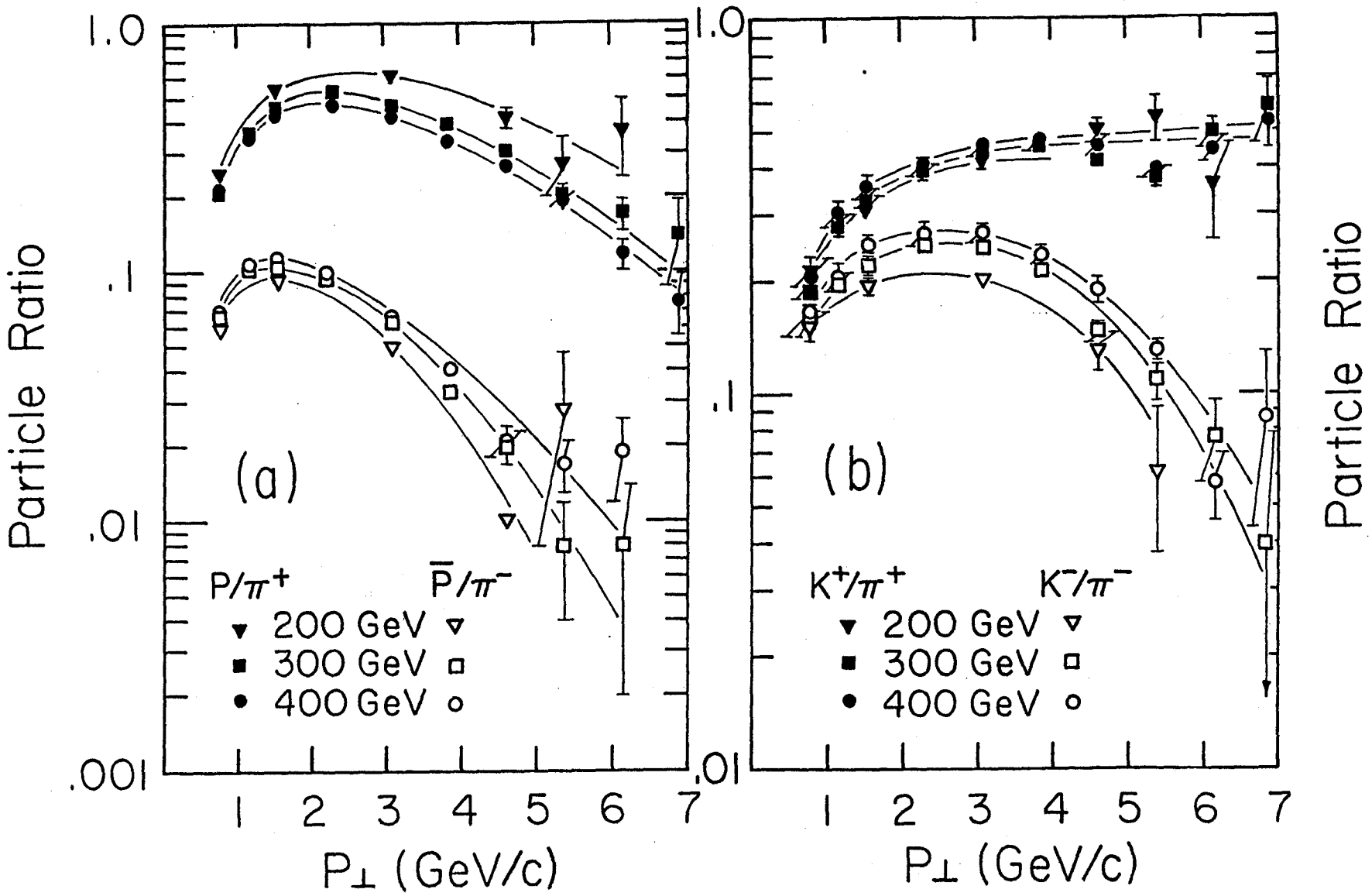
1.0
.1
.01
.001
Particle Ratio
(a)
P/π+
P̄/π−
200 GeV
300 GeV
400 GeV
1 2 3 4 5 6 7
P⊥ (GeV/c)
1.0
.1
.01
(b)
K+/π+
K−/π−
200 GeV
300 GeV
400 GeV
1 2 3 4 5 6 7
P⊥ (GeV/c)
Particle Ratio

FIG. 6.

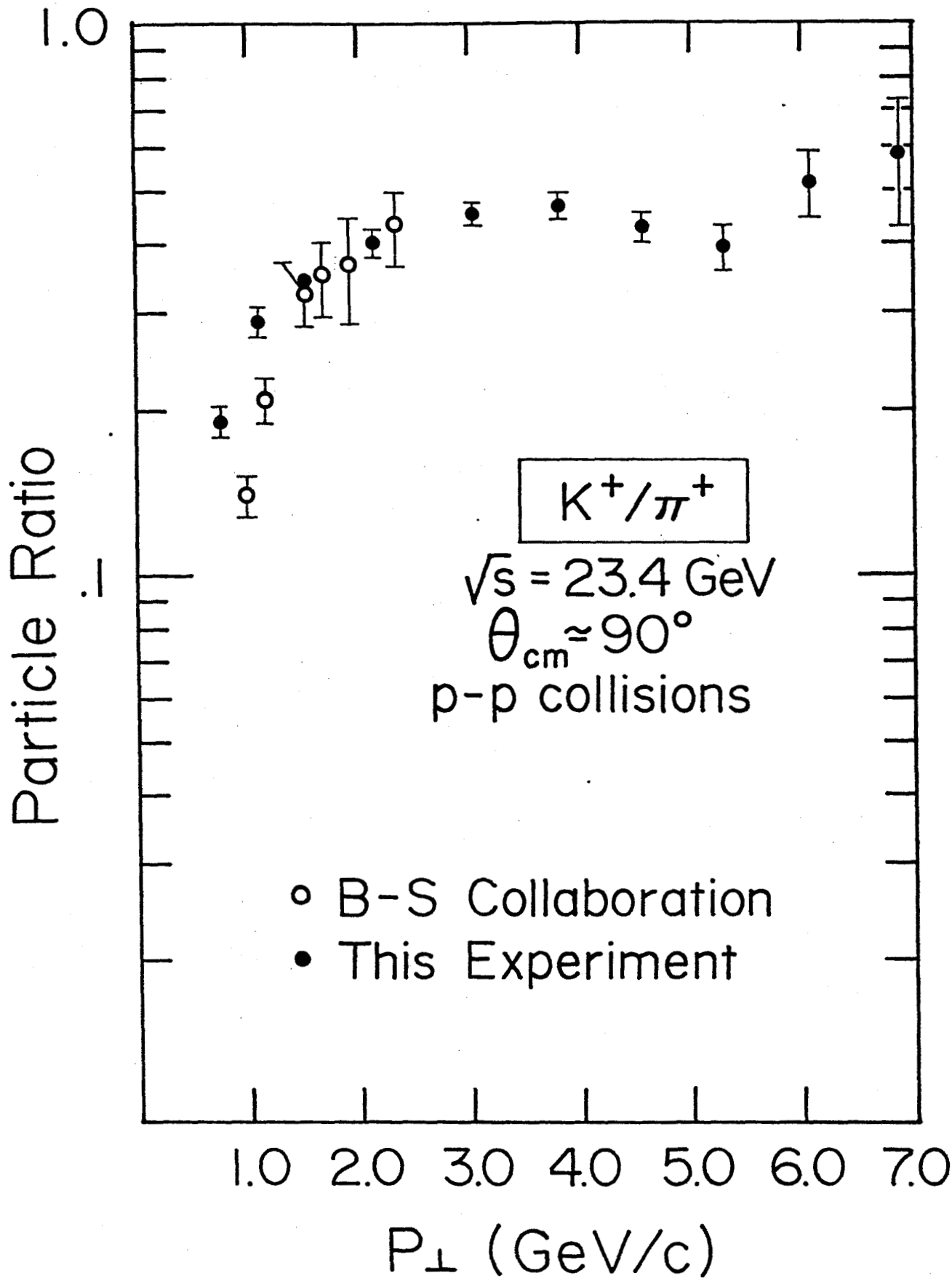
1.0
.1
Particle Ratio
K^+/π^+
$\sqrt{s}$ = 23.4 GeV
$\theta_{cm} \approx 90°$
p-p collisions
o B-S Collaboration
• This Experiment
1.0 2.0 3.0 4.0 5.0 6.0 7.0
$P_\perp$ (GeV/c)

FIG. 7.

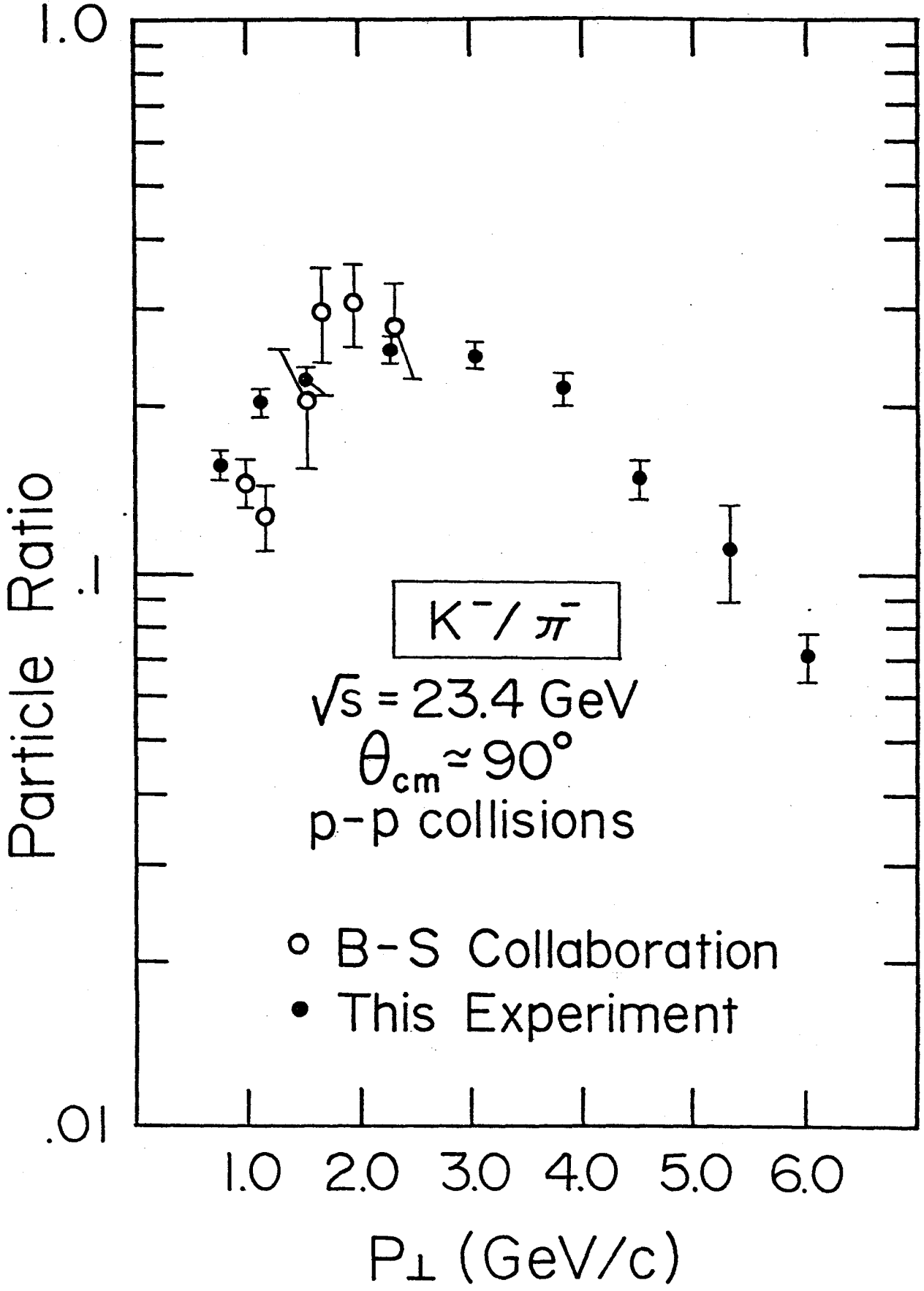
1.0
.1
.01
Particle Ratio
K⁻/π⁻
√s = 23.4 GeV
θcm ≈ 90°
p-p collisions
o B-S Collaboration
• This Experiment
1.0 2.0 3.0 4.0 5.0 6.0
P⊥ (GeV/c)

FIG. 8.

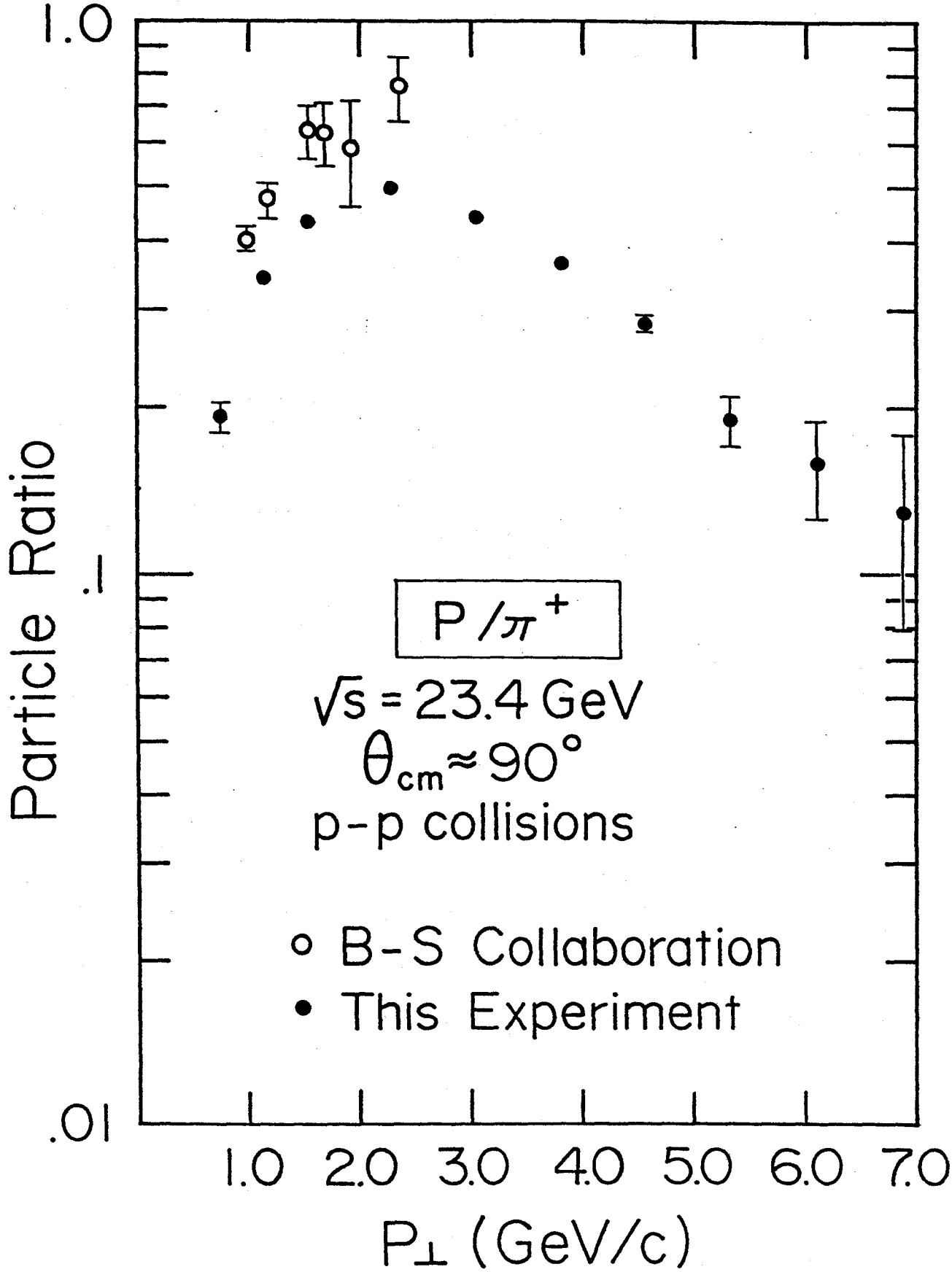
1.0
.1
.01
Particle Ratio
P/π+
√s = 23.4 GeV
θcm ≈ 90°
p-p collisions
o B-S Collaboration
• This Experiment
1.0 2.0 3.0 4.0 5.0 6.0 7.0
P⊥ (GeV/c)

FIG. 9.

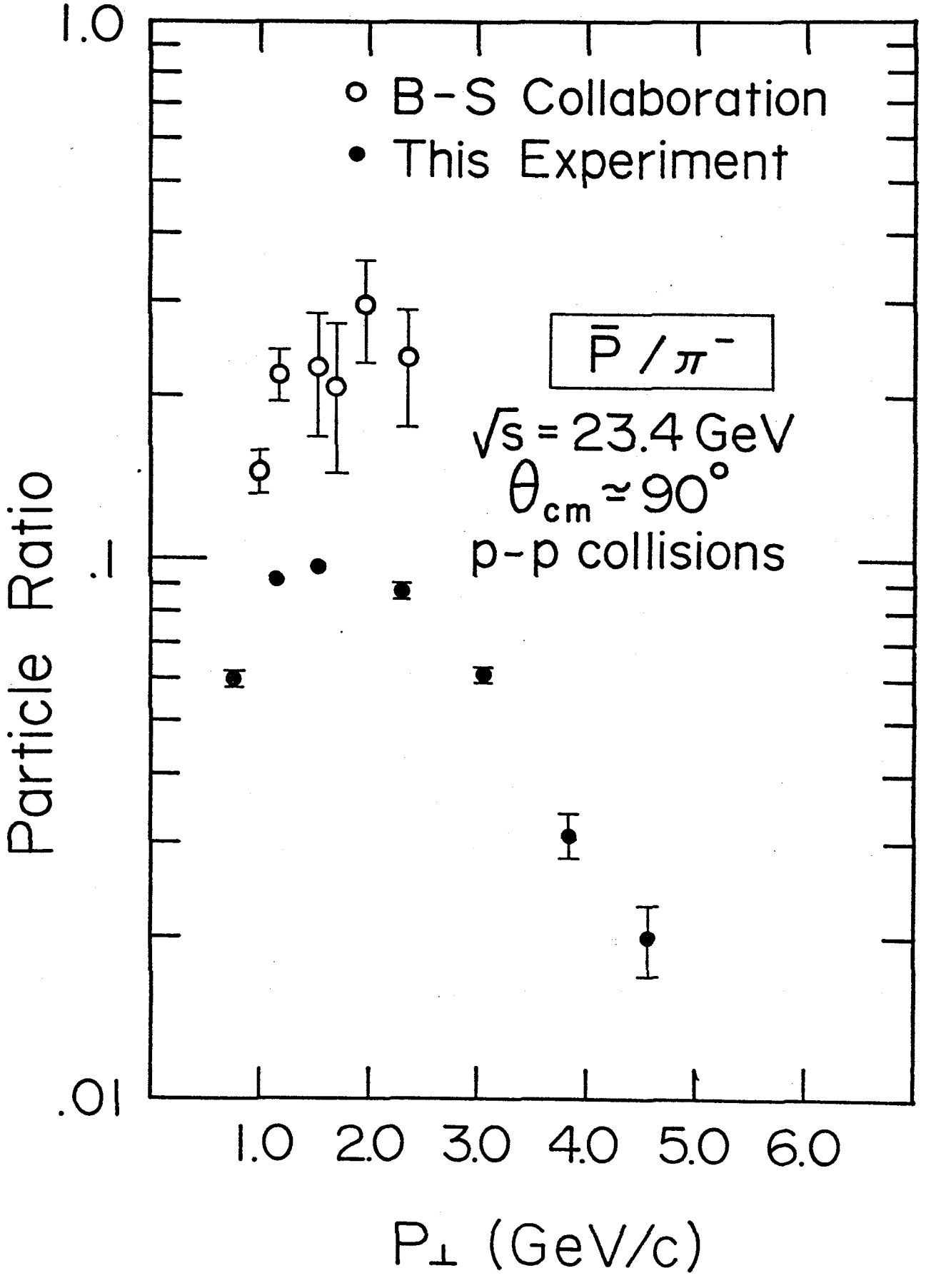
1.0
.1
.01
Particle Ratio
o B-S Collaboration
• This Experiment
$\bar{P}/\pi^-$
$\sqrt{s} = 23.4$ GeV
$\theta_{cm} \simeq 90°$
p-p collisions
1.0
2.0
3.0
4.0
5.0
6.0
$P_\perp$ (GeV/c)

FIG. 10.

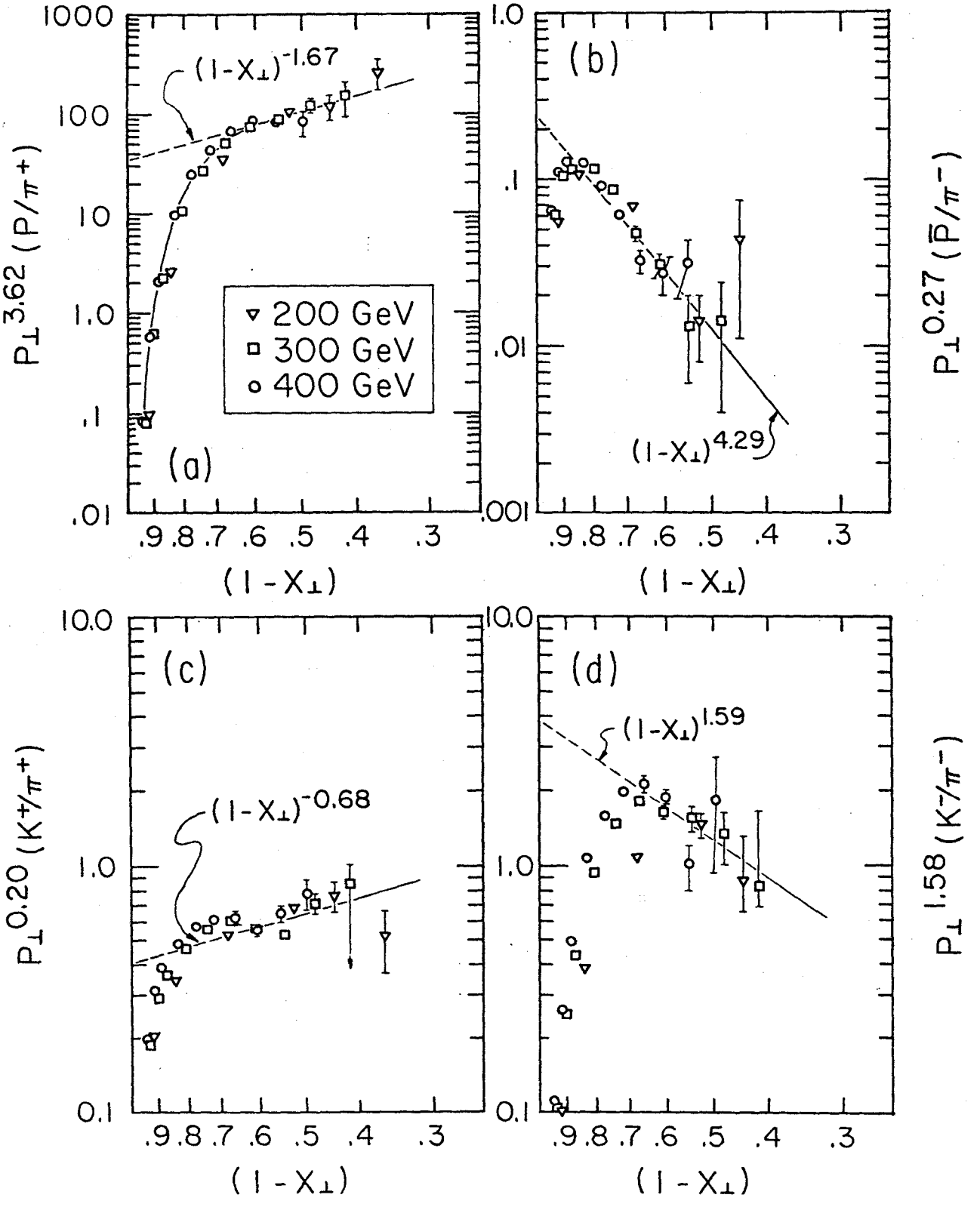
1000
100
10
1.0
.1
.01
$P_\perp^{3.62}(P/\pi^+)$
$(1-X_\perp)^{-1.67}$
200 GeV
300 GeV
400 GeV
(a)
.9 .8 .7 .6 .5 .4 .3
$(1-X_\perp)$
1.0
.1
.01
.001
(b)
$P_\perp^{0.27}(\bar{P}/\pi^-)$
$(1-X_\perp)^{4.29}$
.9 .8 .7 .6 .5 .4 .3
$(1-X_\perp)$
10.0
1.0
0.1
$P_\perp^{0.20}(K^+/\pi^+)$
(c)
$(1-X_\perp)^{-0.68}$
.9 .8 .7 .6 .5 .4 .3
$(1-X_\perp)$
10.0
1.0
0.1
(d)
$(1-X_\perp)^{1.59}$
$P_\perp^{1.58}(K^-/\pi^-)$
.9 .8 .7 .6 .5 .4 .3
$(1-X_\perp)$

FIG. 11.

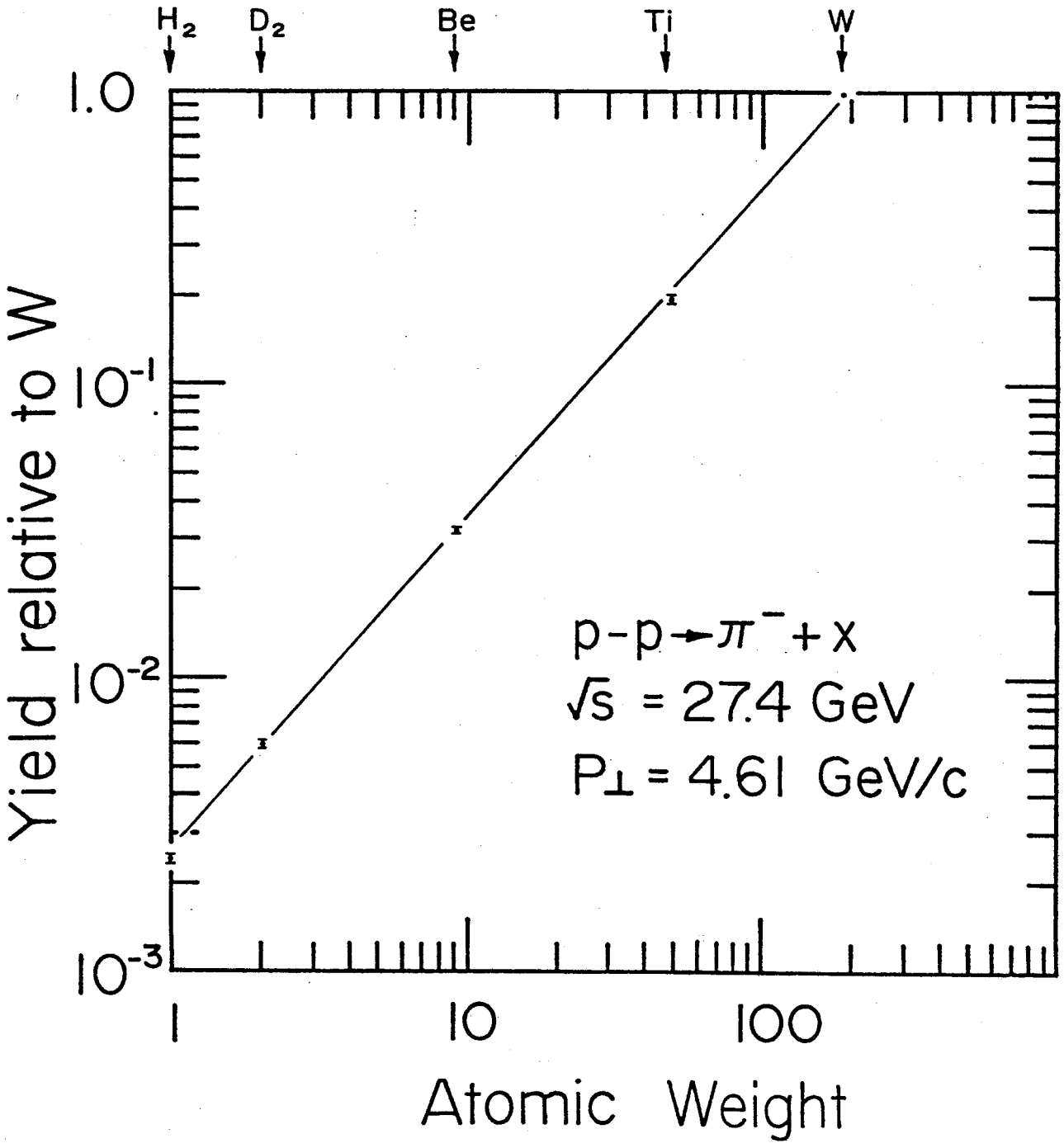
H2
D2
Be
Ti
W
1.0
10-1
10-2
10-3
Yield relative to W
p-p→π⁻+X
√s = 27.4 GeV
P⊥ = 4.61 GeV/c
1
10
100
Atomic Weight

FIG. 12.

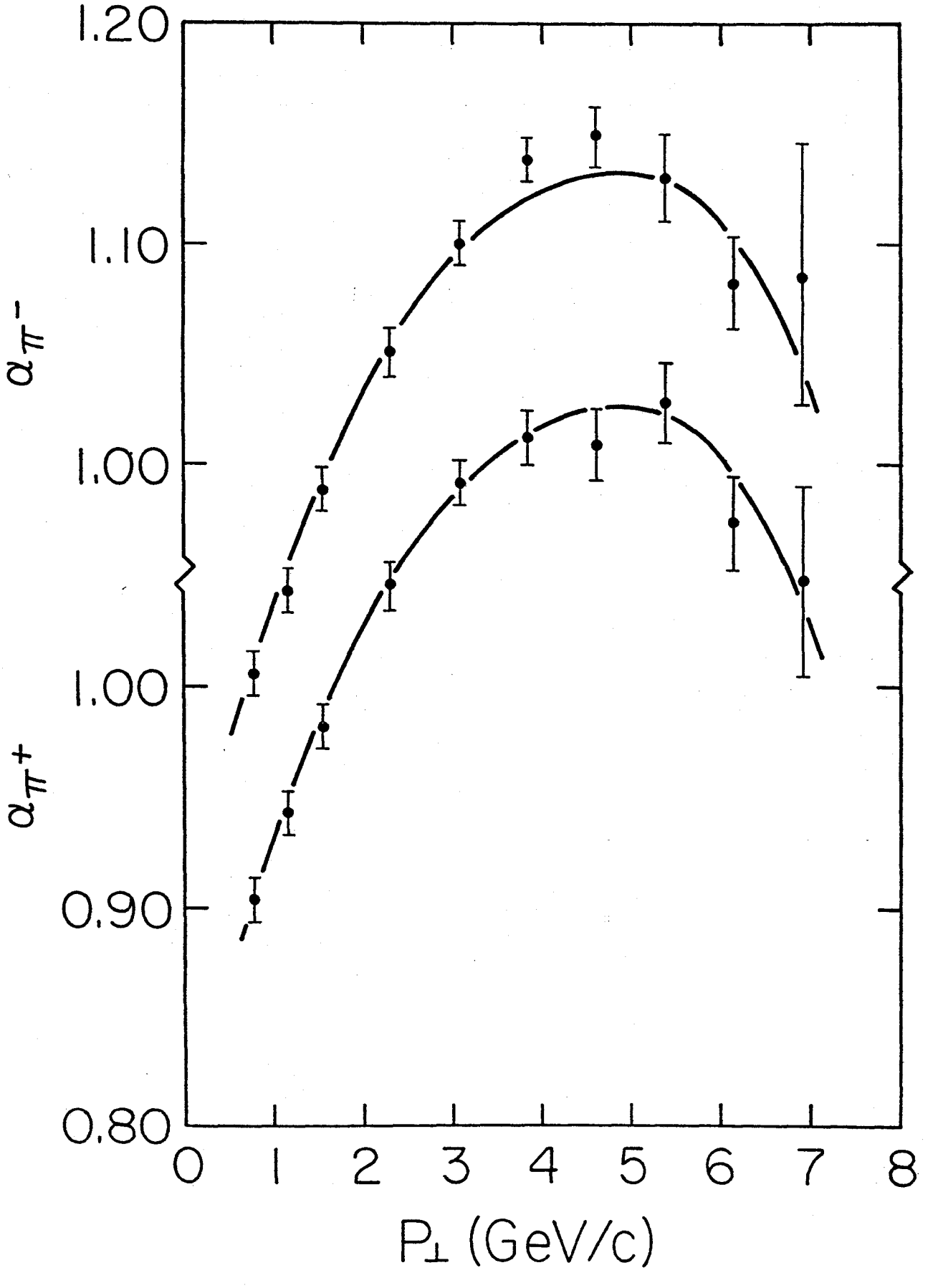
1.20
1.10
1.00
1.00
0.90
0.80
α_{π^-}
α_{π^+}
0
1
2
3
4
5
6
7
8
$P_\perp$ (GeV/c)

FIG. 13.

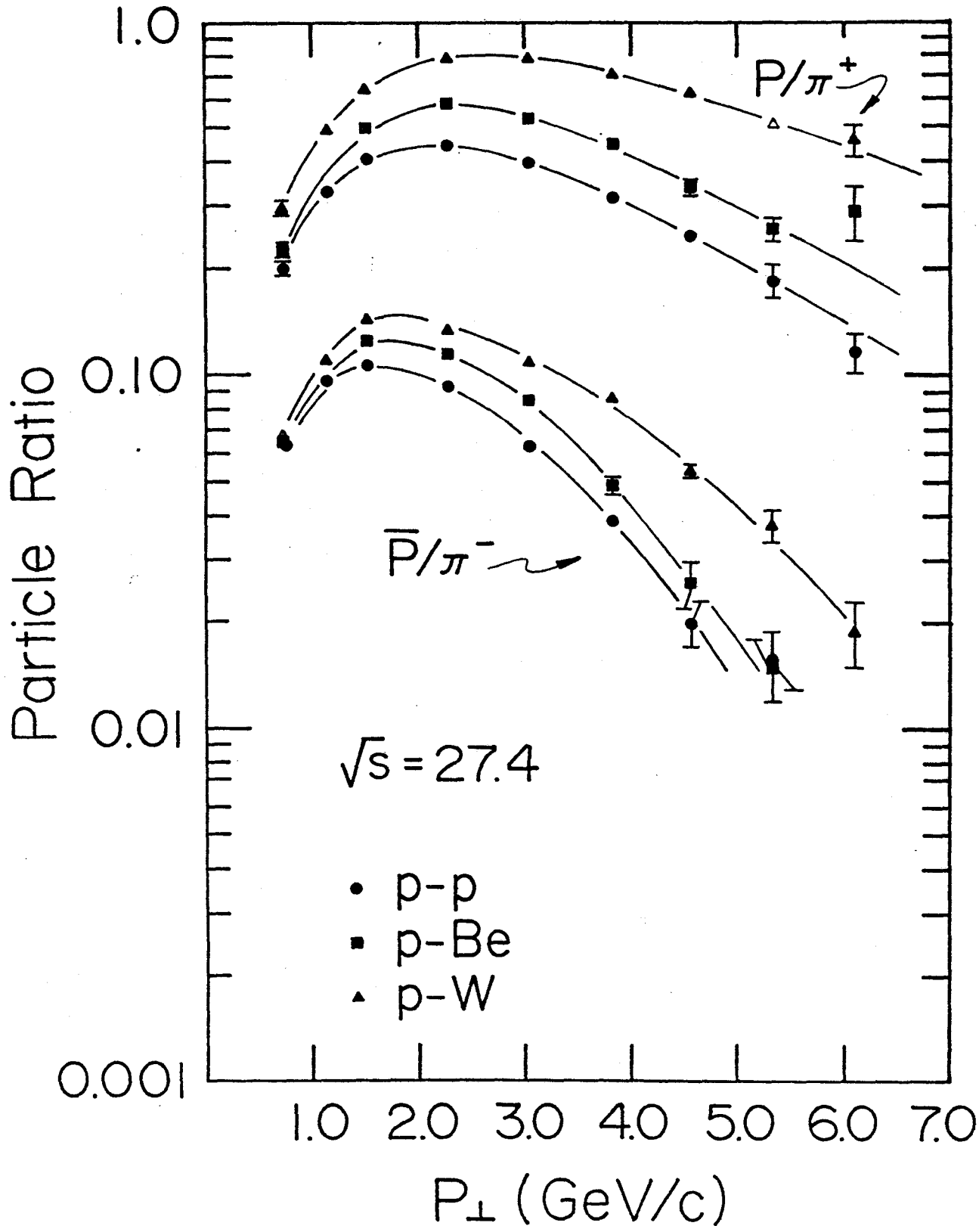
1.0
0.10
0.01
0.001
Particle Ratio
P/π+
P̄/π−
√s = 27.4
p-p
p-Be
p-W
1.0
2.0
3.0
4.0
5.0
6.0
7.0
P⊥ (GeV/c)

FIG. 14.

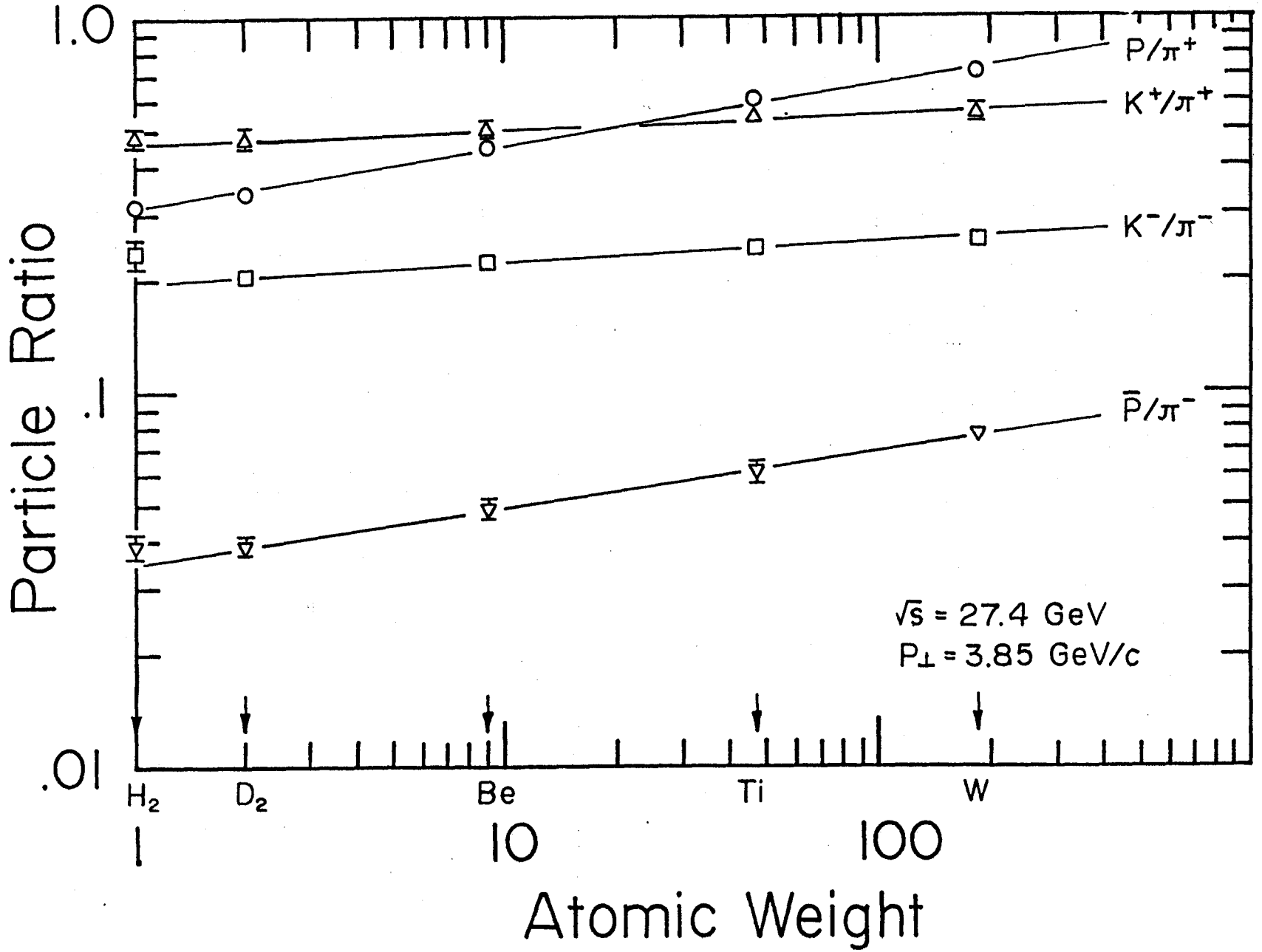
1.0
.1
.01
Particle Ratio
P/π+
K+/π+
K−/π−
P̄/π−
√s = 27.4 GeV
P⊥ = 3.85 GeV/c
H2
D2
Be
Ti
W
1
10
100
Atomic Weight

FIG. 15.

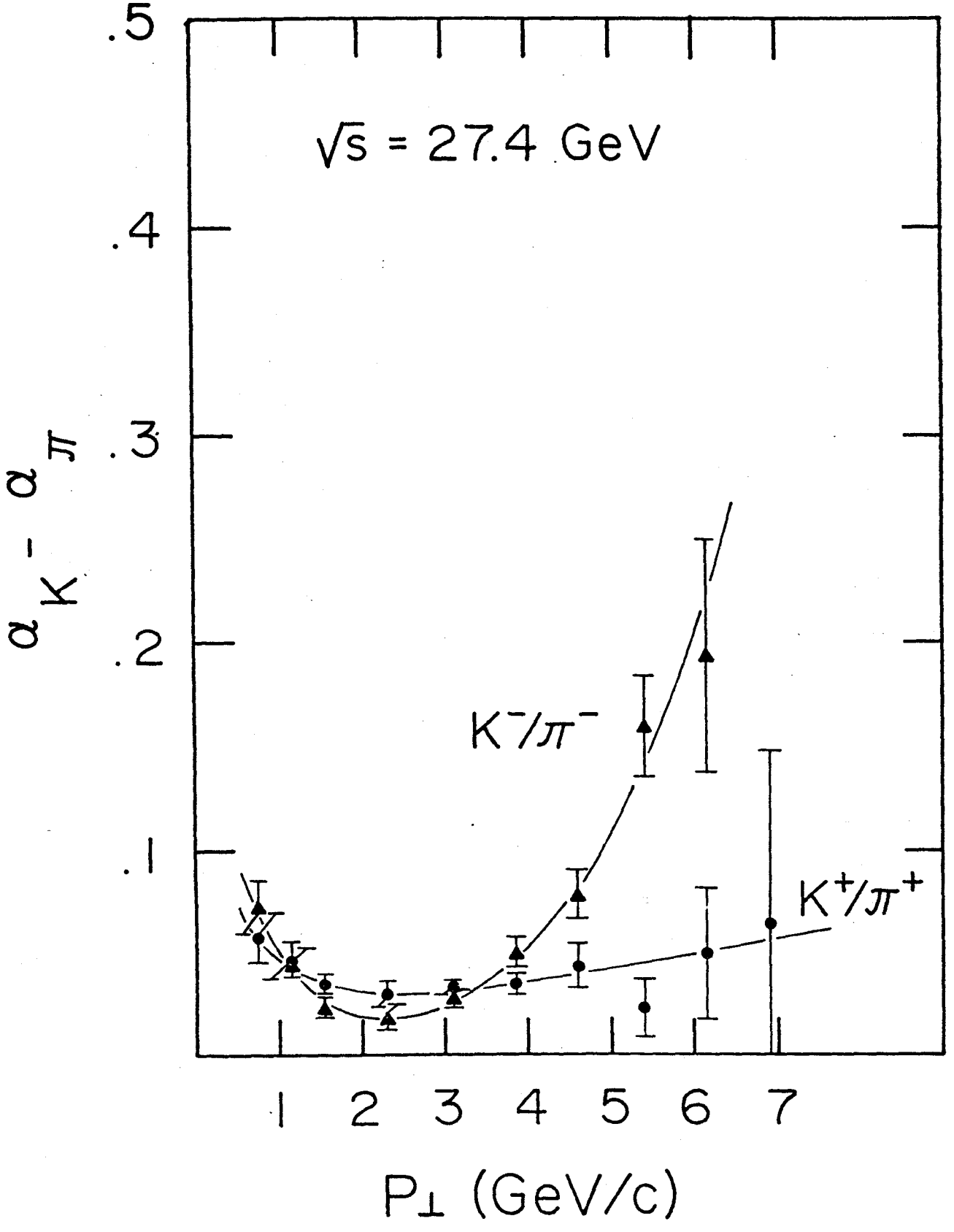
.5
.4
.3
.2
.1
$\sqrt{s}$ = 27.4 GeV
$\alpha_K - \alpha_\pi$
K^-/π^-
K^+/π^+
1
2
3
4
5
6
7
$P_\perp$ (GeV/c)

FIG. 16.

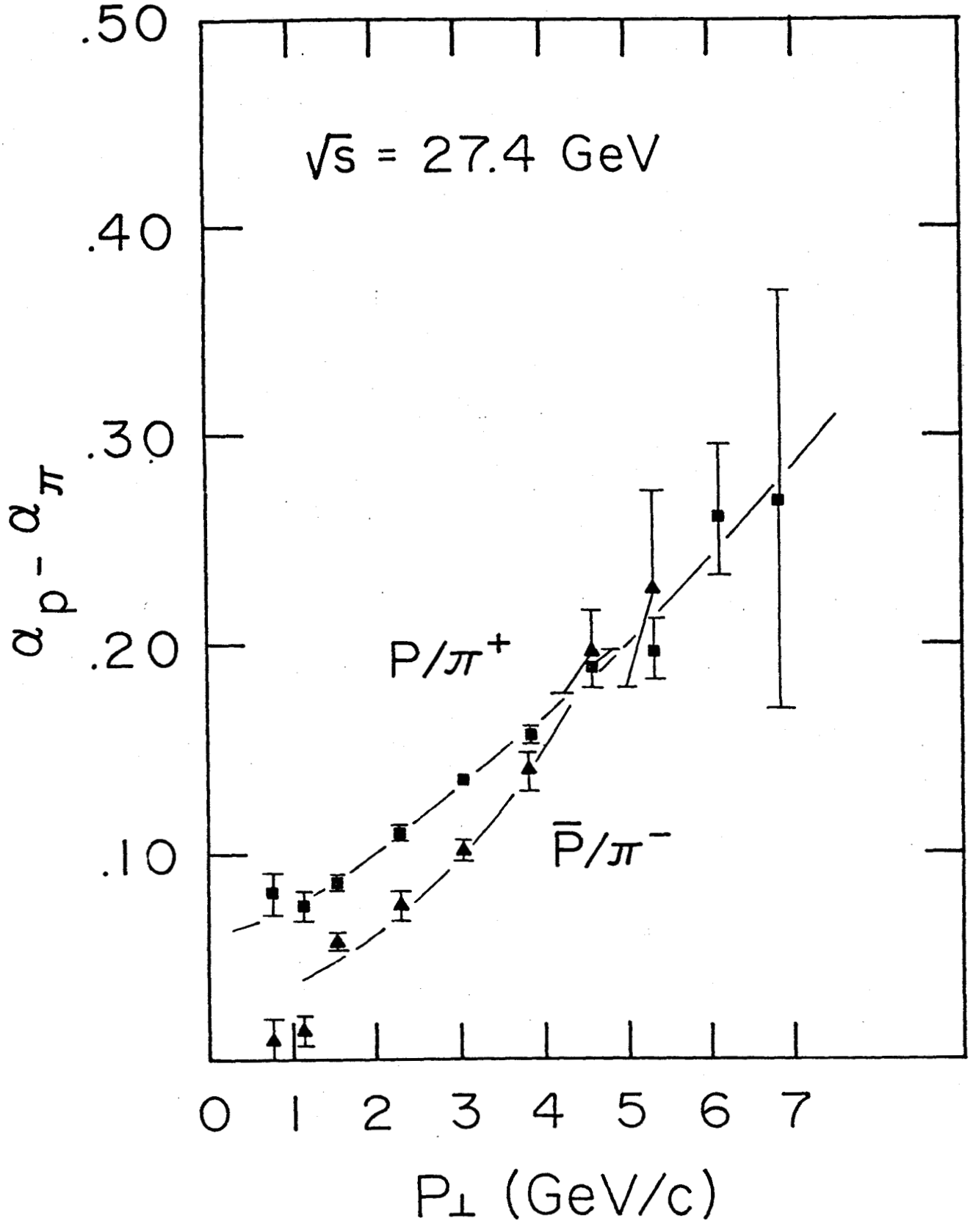
.50
.40
.30
.20
.10
$\sqrt{s}$ = 27.4 GeV
$\alpha_p - \alpha_\pi$
P/π+
P̄/π−
0 1 2 3 4 5 6 7
P⊥ (GeV/c)

FIG. 17.

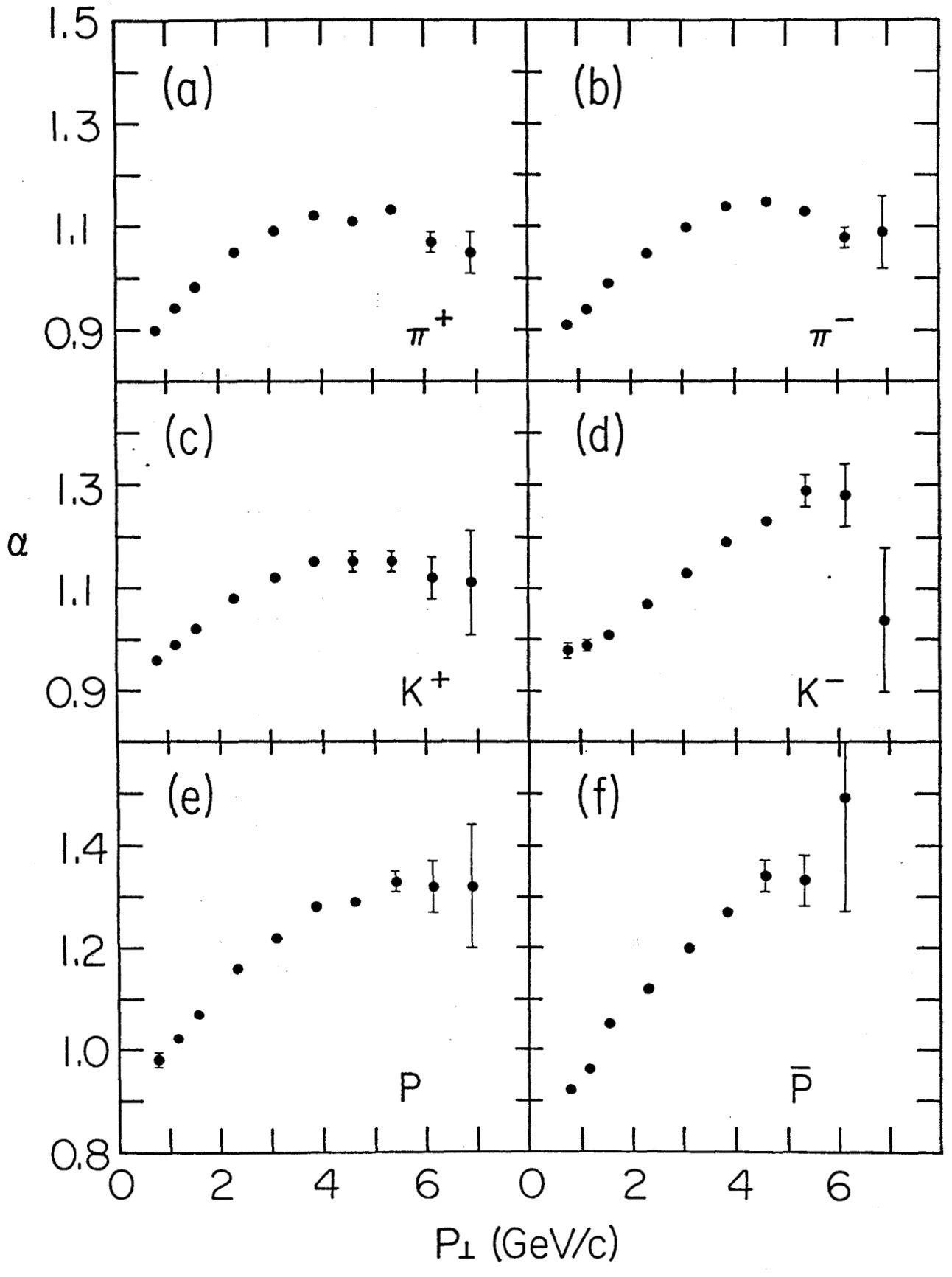

FIG. 18.

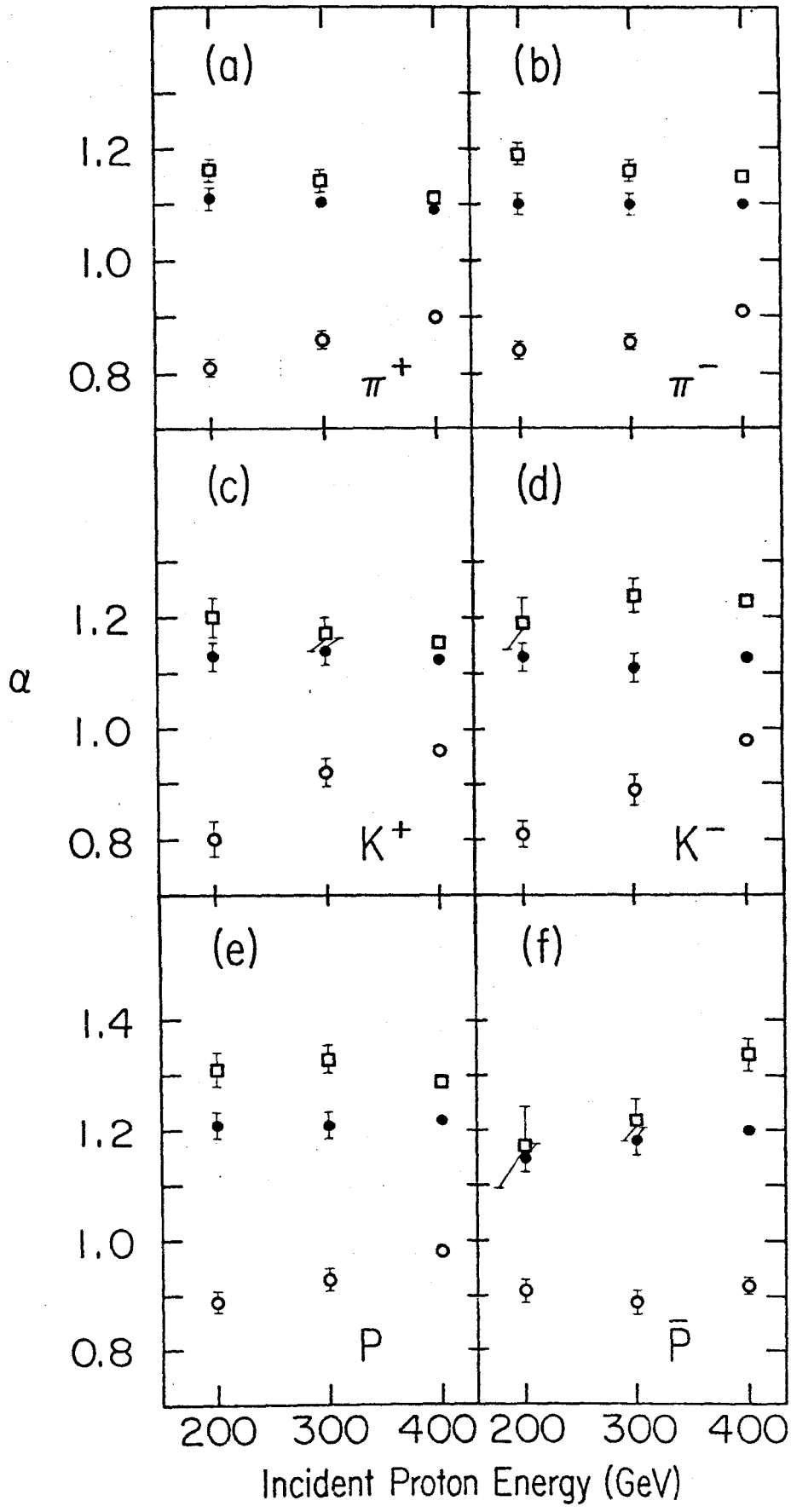
(a)
(b)
(c)
(d)
(e)
(f)
1.2
1.0
0.8
1.4
π^+
π^-
K^+
K^-
P
$\bar{P}$
α
200
300
400
Incident Proton Energy (GeV)

FIG. 19.